Ph.D. Dissertation

Defect engineering of hexagonal boron nitride for electronic applications

February 2023

Graduate School of Seoul National University
Department of Materials Science and Engineering

Younsung Na

Defect engineering of hexagonal boron nitride for electronic applications

Advisor: Prof. Gwan-Hyoung Lee

by
Younsung Na

A thesis submitted to the Graduate Faculty of Seoul National University
in partial fulfillment of the requirements
for the Degree of Doctor of Philosophy
Department of Materials Science and Engineering

February 2023
Approved
by

Chair Ho Won Jang
Vice Chair Gwan-Hyoung Lee
Examiner Hyejin Jang
Examiner Jihyun Kim
Examiner Jangyup Son

Abstract

Hexagonal boron nitride, a 2D insulator with a large band gap (5.5~6.0 eV), has been used in electrical and optical devices that use defects, such as single photon emitters and memristors. Defect controlling and formation are vital because defects are significant components in defining the optical and electrical characteristics of 2D materials. However, the defect has a great effect on the 2D device; there are few studies on the electric-optic properties of hBN induced by the defect.

In this thesis, I systematically investigated the comprehensive properties such as mechanical, optical and electrical of the hBN by using oxygen plasma treatment. I demonstrated that the characteristics of hBN can be controlled using our plasma process. For the first time, I observed a large PL spectrum range of defective hBN using a 325 nm laser. The DFT calculation revealed that the kinds of oxygen-related defects fit well with the PL data. I also demonstrated that plasma-treated hBN's band gap was changed from 5.7 eV to 4.5 eV.

2D materials are easily oxidized and degraded by moisture or oxygen in the atmosphere because the ultrathin has a high environmental sensitivity. Therefore, to fabricate 2D materials-based devices with high device stability and performance, clean interfaces of the 2D channel layer must be achieved through effective passivation. The hBN has been used as a passivation layer for 2D device. Therefore, hBN-encapsulated device requires contact process to connect metal electrode and channel. Various contact processes have been studied, such as edge contact, graphene etch stop, and transferred via contact. However, these process methods have disadvantages such as oxidation, physical damage of 2D channel during device fabrication.

In this thesis, I propose a new contact method for field-effect transistors (FETs) of 2D materials using conductive filament (CF) paths induced by defect. After oxygen plasma treatment on hBN, an electric field was repeatedly applied to form CF paths. As a result, the metal and the 2D channel (graphene and MoS_2) were directly connected. The FETs with CF contacts showed low contact resistance and high stability.

.

Keyword: hBN, oxygen plasma, defect, 2D electronic device, conductive paths, van der Waals heterostructure

Student Number: 2019-37975

Table of Contents

3.1.3 Results and discussions

3.2.3 Results and discussions

Chapter 1. Introduction

1.1. Study Background

The two-dimensional (2D) layered-material has been studied in various research fields such as new physical phenomena and electro-optical devices. The two-dimensional (2D) materials feature covalent bonding inside each sheet as well as van der Waals (vdW) interactions between layers. It can be physically exfoliated into mono- and few-layer nanosheets using the 'Scotch tape' technique.

Andre Geim and Konstantin Novoselov were awarded the Nobel Prize in 2010 for their work in separating monolayers in graphene using scotch tape.(1) Since then, research on various 2D materials, such as graphene, hexagonal boron nitride (hBN), phosphorene and transition metal dichalcogenides (TMDs), has attracted a lot of attention because of the intriguing physical phenomena.(2-5) In particular, research on electro-optical devices using defective 2D materials is under the spotlight. The 2D materials and device performance are affected by defects including charged impurities, strain, vacancy, anti-sites, substitutions, edges and grain boundaries. (Figure 1.1) (6)

Many studies have focused on reducing of defects via encapsulation or synthesis condition control to improve device performance. However, optical and electrical qualities can be modulated by defects. Among the 2D materials, hBN has been used as an insulating and encapsulating substrate due to surface without any dangling bonds or charged traps, flatness, high thermal stability and high thermal conductivity.(7-9) The wide band gap of hBN, 5.5~6.0 eV, allow for the existence of various mid-gap states induced defects. Recently, hBN has been shown to host single photon emitter from point defects with room temperature and the fabrication of resistive random access memory (RRAM) using conductive filament. It means that electrical and optical properties can be modulated by defects.

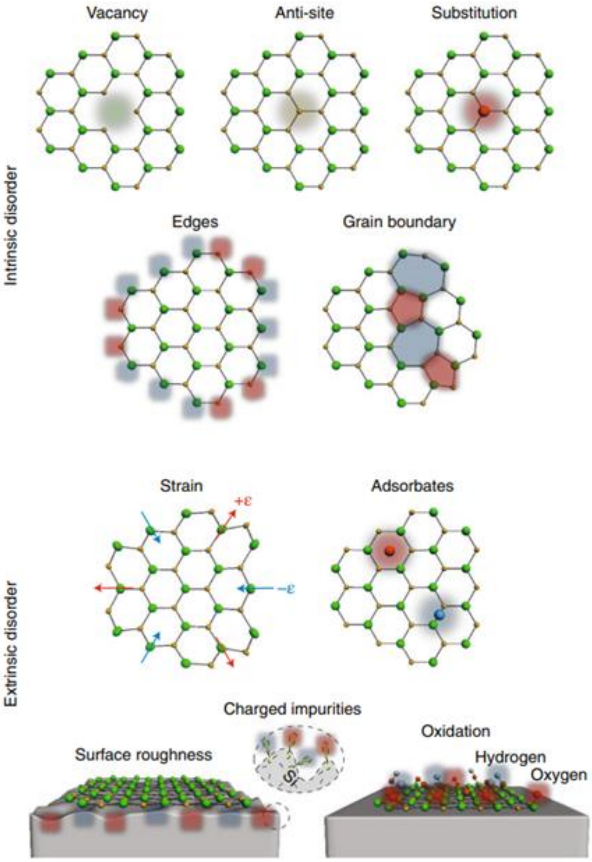

Figure 1.1 Schematic of defect type in 2D materials(6)

1.2. Purpose of Research

Defects in 2D materials can give rise to novel physical phenomena and application possibilities for 2D device. Defect research is significant because defects are crucial elements in changing the electro-optical characteristics of hBN.

The main topic of my thesis is to explore the modulation in the electro-optical properties of defective-hBN and to propose a new contact process by forming CF inside hBN.

In chapter 3-1, I demonstrate the modulation of electro-optical properties through various measurement methods after artificially generating defects in hBN through mild oxygen plasma treatment.

In chapter 3-2, I propose a novel process that direct contacts the metal with the encapsulated channel by forming CFs inside the hBN. Our research demonstrates a novel contact approach with considerable promise for high-performance 2D electronic devices.

.

Chapter 2. General background

2.1. Two-dimensional materials

2.1.1 Hexagonal boron nitride

Hexagonal boron nitride is a two-dimensional (2D) insulating material composed of boron and nitrogen atoms arranged in a honeycomb configuration (Figure2.1).(7, 10, 11) The hBN has a low dielectric constant, great chemical and thermal stability, a clean surface, a high breakdown voltage and a low defect density. Therefore, hBN has been used to fabricate van der Waals (vdW) heterostructures in field effect transistors as an insulating barrier and gate dielectric layer.(12-14)

The surface of an oxide, such as SiO_2 or Al_2O_3, modulates the intrinsic properties of the 2D material by the charge trap and scattering of charge carriers due to dangling bonds and rough surfaces. The hBN has attracted as a new substrate that compensates for the shortcomings of SiO_2, Al_2O_3 substrates. Figure 2.2 shows the graphene device characteristics on SiO_2 and hBN. It was shown that the roughness of graphene transferred on hBN was smaller than that of SiO_2.(15) In addition, when fabricating graphene device using hBN, it shows improved carrier mobility compared to the SiO_2 substrate, indicating that hBN is a suitable material for a 2D material-based insulating substrate.(16)

Further, h-BN encapsulation can provide high device performance and stability of 2D materials-based devices. By encapsulating graphene with hBN, it protects graphene from the local environment and dramatically improves electron transport.(17)

The hBN is a promising material for optical-electrical applications. Recent studies have revealed that a hBN point defect shows single photon emission property from visible to infrared at room temperature.(18) The resistive random access memory (RRAM) device using the insulating property and conductive path of hBN has gained interest. Deji and co-workers reported the thinnest RRAM device with stable and large on/off ratio 10^7. (19)

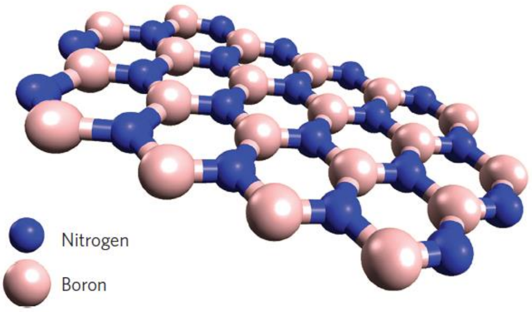

Figure2.1 Schematic illustration of a hBN monolayer.(18)

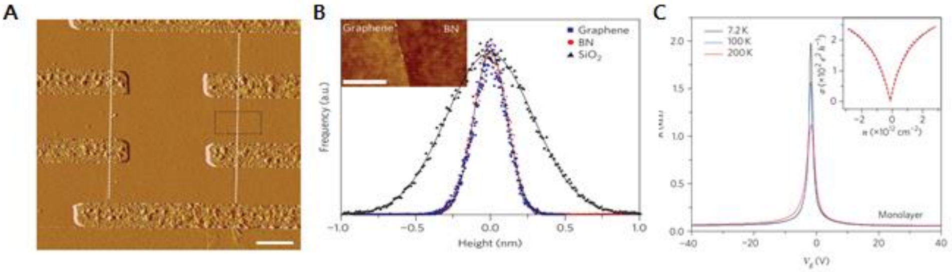

Figure2.2 (A) AFM image of graphene on SiO_2 and hBN substrates.(B) Histogram of the height distribution (C) Resistance versus applied gate voltage for monolayer graphene(15)

2.1.2 Transition metal dichalcogenides

Two-dimensional materials have been explored in a wide range of fields since the advent of graphene. Although graphene presents superior properties, the lack of a band gap limits the applicability of electro-optical devices.

Accordingly, many studies on electro-optical devices using 2D materials with semiconductor properties, such as MoS_2, WSe_2, have been reported. Transition metal dichalcogenides (TMDCs) are semiconductor of the MX2 type, which are composed of a transition metal atom (M or W) and a chalcogen atom (S, Se or Te) as shown in Figure 2.3A. Each atom in these materials has a strong covalent bond, and the interlayer has a van der Waals (vdW) interaction.(20)

TMDCs exhibit unique properties such as band structure transition on depending on its thickness, band gab, mechanical and strong spin–orbit coupling.

The MoS_2 is one of the most extensively studied TMDCs materials. MoS_2 has an indirect transition characteristic in a bulk form and its band gap is 1.2 to 1.3 eV. However, when MoS_2 is thinned down to monolayer thickness, its band gap is 1.8~1.9 eV in direct band gap due to quantum confinement effect. (Figure 2.3B)(21) MoS_2 FET device show high mobility (200 cm2/V•s) and on/off ratio 10^8.(22) This results showed the possibility of application to electronic devices.

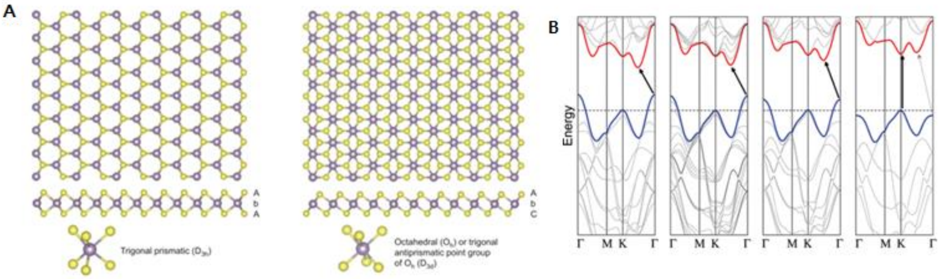

Figure 2.3 (A)Structure of monolayered TMDs.(purple: metal, yellow: chalcogen) (20) (B)Band structure of MoS_2 according to thickness(23)

2.2. Van der Waals heterostructures

2.2.1 Stacking techniques for van der Waals heterostructures

The family of 2D materials consists of semi metal, semiconductor and insulator. Owing to ultraclean interface, these materials can be combined to form vertical vdW heterostructures. This structure can show unprecedented characteristics or unique functionalities because the properties of each material are different. Therefore, stacking strategies for building van der Waals (vdW) heterostructures have been devised.. Here some techniques are introduced for transferring 2D materials.

Wet transfer is the most commonly used method to transfer 2D materials. This method creates a vdW structure using PMMA and transfer film.(16) First, water soluble layer and PMMA are coated substrate (Si/SiO_2), and then 2D flakes are exfoliated on it. Second, to separate the second substrate (Si/SiO_2) from the PMMA/2D flake, dip the substrate slowly in water. The soluble polymer is dissolved and then the substrate (Si/SiO_2) and PMMA/2D flakes are separated. During this process, PMMA serves to protect the 2D flakes from physical damage. PMMA/2D floats on water because of its hydrophobic properties. The PMMA/2D material on the water is scooped out with a PDMS-attached slide glass (2D/PMMA/PDMS/glass). This slide glass is aligned with different 2D flake positions using a microscope to make contact. PMMA is melted through an annealing process. Then, the PDMS is removed from the substrate (PMMA/2D/another 2D/SiO_2/Si), and finally, the heterostructure is immersed in the solvent to dissolve the PMMA. (Figure 2.4A)

The advantage of this technology is that it reduces mechanical damage to 2D materials. However, it is difficult to completely remove the PMMA remaining on the 2D material surface. This PMMA residue deteriorates the electro-optical device characteristics of the electronic device. To solve this problem, Dean *et al* proposed an improved dry transfer method.(24) This is a method of pick- up 2D materials one by one using a polypropylene carbonate (PPC) film and PDMS as a carrier film. To increase the adhesion of the PPC film and the vdW structure, it is maintained at 40 degrees during the pick-up and transfer process. Then, the temperature is raised to 90 degrees to release the PDMS. Finally, the ppc film is removed by acetone to obtain a heterostructure. The TEM cross-sectional diagram of the structure to be made using this method, a very clean and sharp interface can be confirmed as shown in Figure 2.4B. This method is a method that can reduce the residue head on the surface of a two-dimensional material.

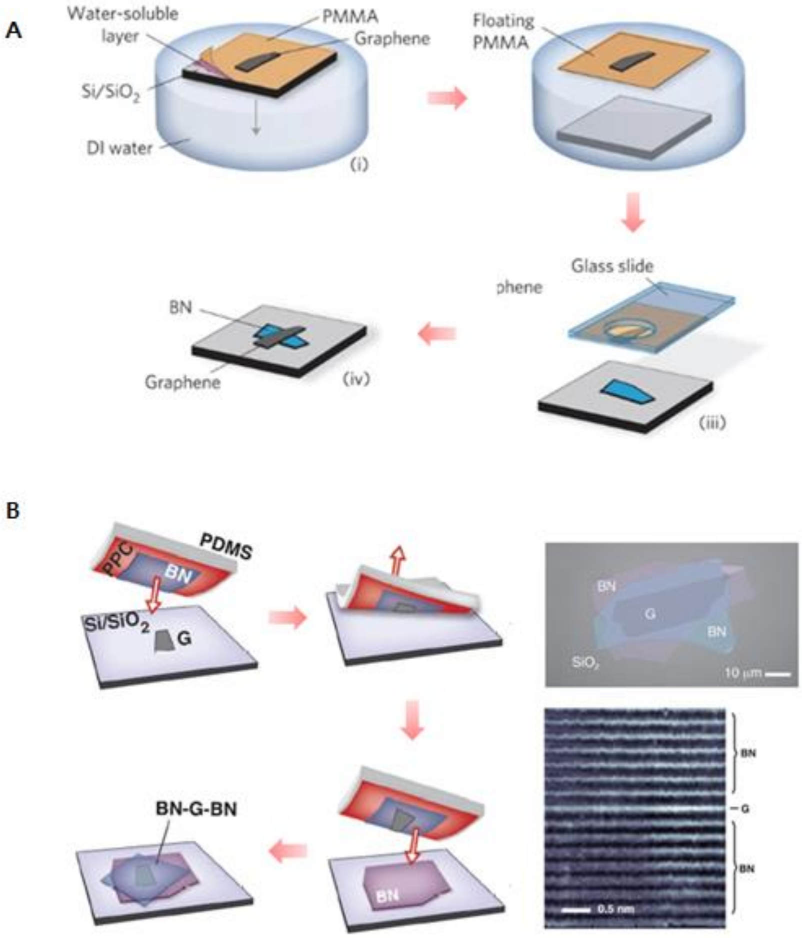

Figure 2.4 (A) Wet transfer method(16) (B) Dry transfer method(24)

2.2.2 Encapsulation effect by hexagonal boron nitride

Due to their superior electrical characteristics, such as high carrier mobility and improving the short channel effect, two-dimensional (2D) materials are intriguing candidates for next-generation materials for electronic devices.(25-27) However, 2D materials occurs in unintentional doping or degradation by polymer residues during fabrication process and active species in ambient atmosphere.(28) Effective passivation of 2D materials is critical for clean channel layer interfaces in order to achieve high-performance and reliable devices.. Among the many passivation materials for 2D-based device, hexagonal boron nitride (hBN) of 2D insulator is an ideal material, as it has impermeability to water and oxygen, good thermal dissipation and boosting electrical performance of active layer.(29, 30) Accordingly, a 2D stacking technology that can construct the hBN-based van der Waals (vdWs) heterostructure has been developed, and the vdW heterostructure which can be integrated vertically has a high potential for application in nano-device.(31-34)

Figure 2.5 shows the changes in Raman shift and PL when exposed to various environments to confirm the environmental stability of the hBN-encapsulated MoS2 device. As shown in Figure 2.5, there was almost no change in the air for 8 months. These results show that hBN is an excellent passivation material.(35)

The vdW heterostructure MoS_2 device entirely encapsulated hBN layer shows the high device stability under ambient condition. Figure 2.6 shows the transfer curve of the MoS_2 using encapsulated with hBN. Up to 2 months, MoS_2 device performance is unchanged, while un-encapsulated MoS2 device shows significantly decrease of mobility.

Figure 2.7 shows the charge inhomogeneity in graphene devices. When graphene is on the hBN substrate, the charge inhomogeneity is significantly reduced compared to SiO_2 graphene device because hBN has much better crystallinity than SiO_2. Moreover, it can be seen that charge fluctuation is more effectively suppressed when graphene is completely encapsulated with hBN.(36)

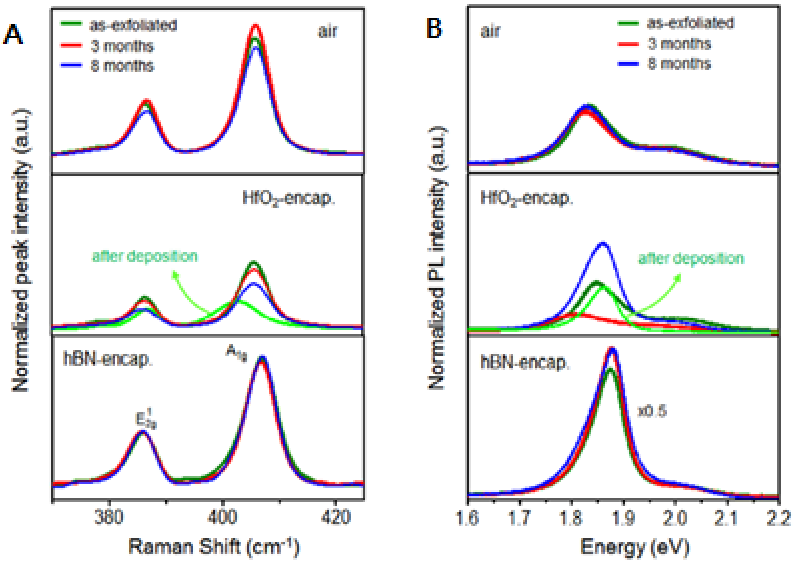

Figure 2.5 (A) Raman and (B) photoluminescence (PL) spectra of monolayer MoS$_2$ over 8 months (35)

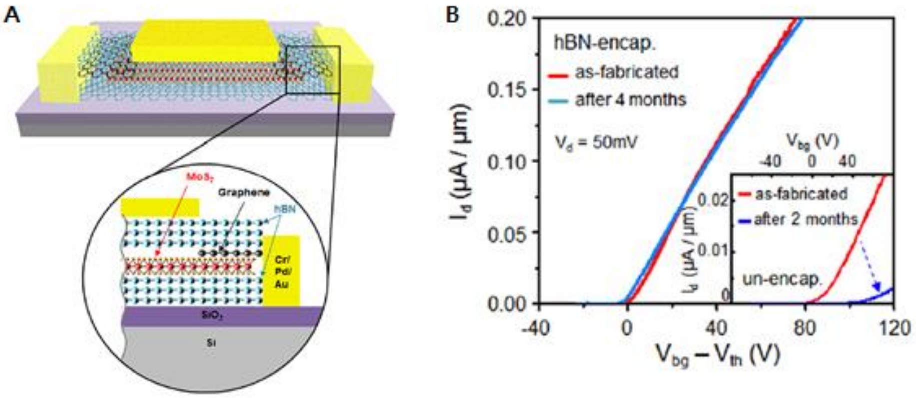

Figure 2.6 (A) Schematic of hBN-encapsulated MoS_2 field-effect transistor contacted with graphene electrodes (B) Transfer curve of the hBN-encapsulated MoS_2 device without degradation over 2 months (35)

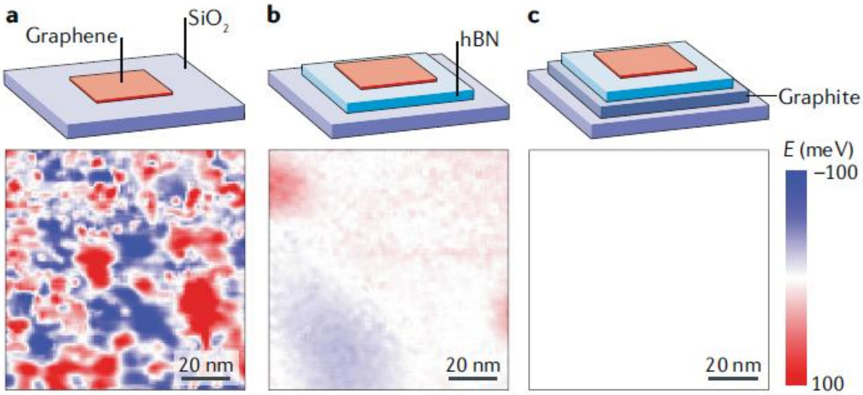

Figure 2.7 Charge fluctuations of graphene on SiO_2 and hBN(36)

2.2.3 Contact strategies for vdW heterostructure devices

Since the 2D material is sensitive to the external environment due to its thin thickness, it is necessary to encapsulation process with an excellent insulating material. As connection between metal electrode and embedded channel layer is essential in passivated vdW heterostructure, various contact methods have been proposed. Here I introduce contact methods in various passivated device structures.

Edge contact was invented, in which metal electrodes only make contact with the exposed lateral edges using lithography and etching.(37, 38) Edge contact based on graphene channel was reported for the first time, and it was developed as a hybrid contact in which the vdWs and edge contacts based on graphene electrode with transition metal dichacogenide (TMD) channel are combined.(24, 39) (Figure 2.8) This contact method allows graphene and metal to contact in 1D through an etch process. Since graphene and metal are 1D contact, although carrier injection is a limit, it shows a notable low contact resistance.

However, it has high contact resistance (Rc) due to oxidation on terminated edge during etching.(40-42) The edge contact technique still has many issues to solve such as challenging fabrication process, high Rc due to the small contact area and damage to the lower substrate via etching process.

Another method is fluorinated graphene via contact using graphene etch stop (GES) technique with XeF_2 gas, as described in Figure 2.9 (43) Although this technology was a first demonstration of 3D integration using 2D via contact, it is possible with only graphene rather than other 2D materials.

Recently, transferred via contact, metal-predeposited hBN was transferred onto a

TMD, was demonstrated.(44). Figure 2.10 shows fabrication process for TVCs and conventional contacts. The technique with vdWs contact can suppress the Fermi-level pinning effect and exhibited high hole mobility and low contact resistance through WSe_2 FET. However, the transfer method is not easy to align concisely when implementing the nano-device. During the transfer process, the process was performed in a glove box to prevent oxidation of the metal.

The contact methods have been introduced for encapsulated 2D device. However, there are still challenges to be solved. A new approach on contact method in passivated vdW heterotucture is required.

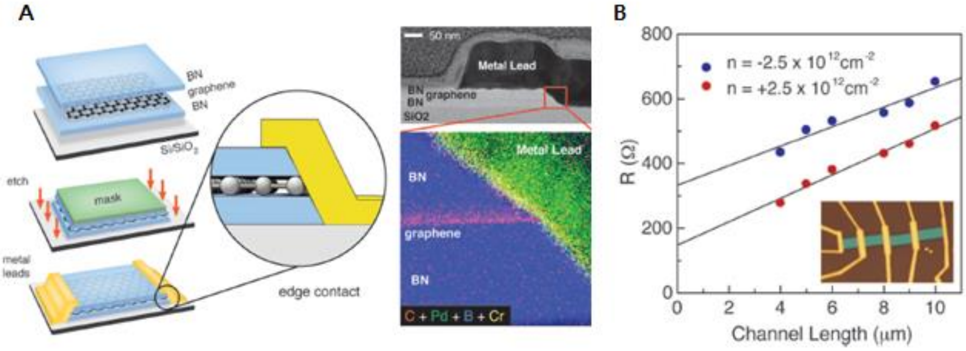

Figure 2.8 Charge fluctuations of graphene on SiO_2 and hBN(39)

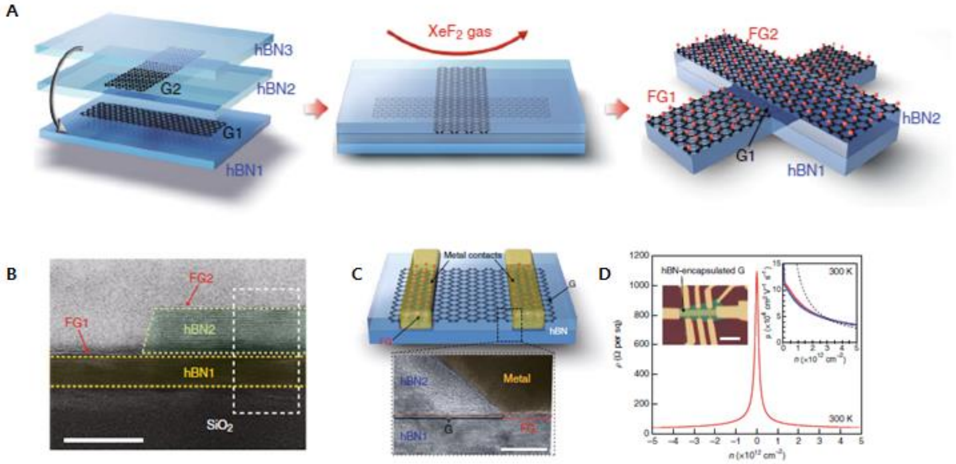

Figure 2.9 (A) Graphene etch stop process (B) STEM image of the etched heterostructure (C) Schematic of a hBN-encapsulated graphene device with FG via contacts (D) Resistivity as a function of carrier density at room temperature(43)

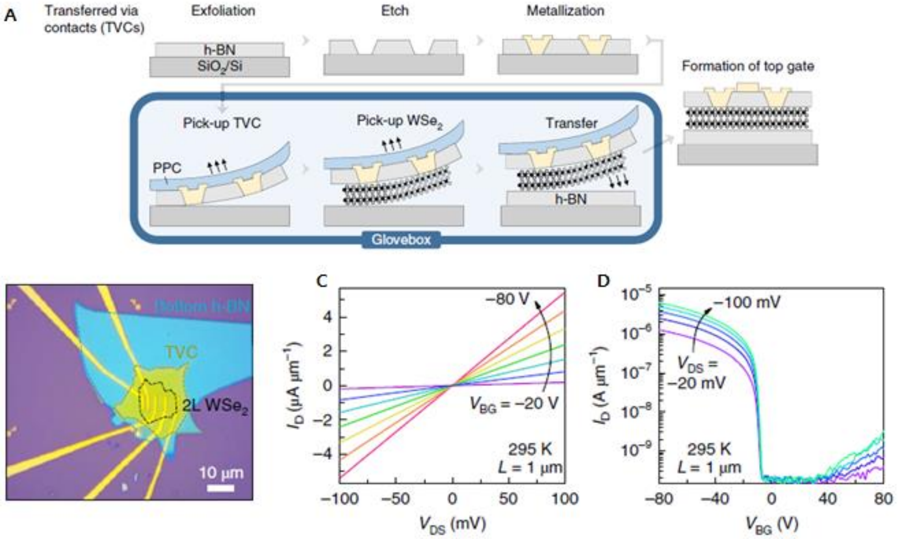

Figure 2.10 (A) Fabrication process for transferred via contact (TVC) (B) Optical microscope image of WSe_2 FET device using TVC contact (C,D) Electrical properties : output(C), transfer curve(D) (44)

* This chapter has been published in a journal. Manuscript is reproduced with permission from Na et al., *2D Mater*. 8 (2021) 045041

Chapter 3. Defect engineering for hexagonal boron nitride

3.1. Modulation of electrical and optical properties of hBN

3.1.1 Introduction

Hexagonal boron nitride (hBN), a two-dimensional (2D) insulating material with a wide band gap (5.5-6.0 eV) has drawn much attention as used for the ideal insulating substrate and tunnel barrier for 2D materials transistor that are benefited by the absence of dangling bond, high crystalline quality, and thermal stability.(7, 36, 45-47) Recently, defects of hBN have been used for electrical and optical devices, such as single photon emitters and memristors.(18, 19, 48, 49) Many studies have been conducted to characterize the devices employing hBN defects and induce them by various methods, such as laser ablation (50), ion/electron irradiation (51), and chemical etching (52). However, little attention has been paid to the study on the modulation of optical and electrical properties of hBN induced by defects in spite of the large effect of defects in the performance of 2D heterostructure devices. Here, I investigate how the plasma-induced defects of hBN modulate its intrinsic optical and electrical properties. The oxygen plasma treatment generates the oxygen-related defects in the crystal structure of hBN, which lead to the increased photoluminescence (PL) intensity depending on the energy levels and amounts of defects within the large band gap of hBN. The insulating barrier of plasma-treated hBN decreases significantly due to the defect-induced conductive paths. In addition, photoemission spectroscopy (PES) measurement exhibits a bandgap narrowing due to the disordered structure of plasma-treated hBN**.**

3.1.2 Experimental procedure

Sample preparation: The hBN flakes were mechanically exfoliated on the 285 nm-thick SiO_2/Si substrates. Oxygen plasma treatment was carried out on the hBN flake using a reactive ion etch (RIE) mode (Femto Science, CUTE). The treatment parameters are as follows: RIE power (100 W), frequency (100 kHz), pressure (10-1 Torr), O_2 flow rate (20 sccm), and treatment time (1 - 31s). The as-exfoliated and plasma-treated hBNs were transferred onto Au-coated SiO_2 substrates for the conductive atomic force microscopy (c-AFM), Kelvin probe force microscopy (KPFM), photo-emission spectroscopy (PES), and near-edge X-ray absorption fine structure (NEXAFS) measurements.

Material characterization: The as-exfoliated and plasma-treated hBNs were examined by Raman spectroscopy with a 325 nm He-Cd laser (Horribar Jovin Yvon, LabRAM ARAMIS). The AFM (Park System, NX-10) was used to measure the friction force microscopy (FFM), c-AFM and KPFM in ambient conditions. For contact modes (FFM and c-AFM) and non-contact mode (KPFM), a soft-tip coated by Pt (Nanosensor, PPP-CONTSCPT) was used under the fixed loading force of ~3 nN. For the c-AFM measurements, a specimen was mounted on a metallic sample holder, and an external current amplifier (FEMTO, DLPCA-200) was used to measure the extremely low current. The cross-section transmission electron microscopy (TEM) and electron energy loss spectroscopy (EELS) analysis was conducted using a Cs-corrected TEM (JEOL, JEM-ARM200F) at 80 kV. PES and NEXAFS spectra were measured at 4D and 8A beam line at Pohang Accelerator Laboratory. The NEXAFS spectra were obtained with partial electron yield at a 45 low current. The cross-section transmission electron microscopy (TEM)

Computational method: To comprehend the PL, I performed the first-principles calculations based on density functional theory (DFT). I used a hexagonal unit cell, which is 8 × 8 ×1 supercell of the primitive unit cell of hBN. The lattice constant in the in-plane direction is 20.08 Å, and the vacuum between two planes is 10 Å. All the calculations are performed using the Vienna Ab initio Simulation Package (VASP) (53) with Perdew-Burke-Ernzerhof (PBE) (54) functional to optimize the geometric structures and the screened hybrid HSE06 functional to obtain the more accurate energy gaps between two defect states. The valence electrons were spanned by the plane-wave basis with the cut-off energy of 500 eV, and the projector augmented wave potentials were employed (55, 56). The Brillouin-zone was sampled only by the Γ-point and the positions of atoms are optimized with a force tolerance of 0.01 eV/Å.

3.1.3 Results and discussions

3.1.3.1 Structure of plasma-treated hBN

The hBN flakes were mechanically exfoliated with a scotch tape on a SiO_2 (285 nm)/Si substrate. The conventional plasma tools operating at high frequency vigorously etch ultrathin 2D materials, which are too harsh to generate a small number of defects .(57) I used customized plasma equipment to gently generate defects of low density on the hBN surface. (58) Our plasma system (pressure = 0.1 ~ 1 Torr and adjustable working frequency = 100 kHz) enables us to precisely control the defect concentration of hBN due to minimized ion bombardment. To investigate the structural change of plasma-treated hBN, I used Raman spectroscopy with a high-energy laser of 325 nm wave length. Figure 3.1.1(a) displays the Raman spectra of plasma-treated hBN for different duration. The characteristic peak of hBN was observed at 1366 cm-1, which corresponding to the E2g phonon mode.(59) There was no recognizable change in position and full-width-at-half-maximum (FWHM) of the Raman peak even after plasma treatment for 31 s as shown in Figure 3.1.1(b). The thickness and surface roughness of the plasma-treated hBN were measured by AFM in Figure 3.1.1(c). The thickness of the hBN was reduced by 0.4 nm after the oxygen plasma treatment of 14s, corresponding to etching rate of 1.7 nm/min. The roughness of both as-exfoliated and plasma-treated hBNs showed a comparable value of ~0.3 nm. To measure the friction of the plasma-treated hBN, I used FFM. Friction measurements of as-exfoliated and plasma-treated hBN in Figure 3.1.2 show that the friction increased right after the oxygen plasma treatment regardless of treatment time due to the B-N bond breaking and oxygen chemisorption on the surface of hBN.(60) The longer plasma treatment showed no increase in friction. Even though there is no recognizable change in Raman spectrum of plasma-treated hBN, there is clear change in the friction. This result implies that our plasma treatment induces a small number of defects in hBN. However, to verify the type and position of defects in hBN, I conducted further investigations as follows.

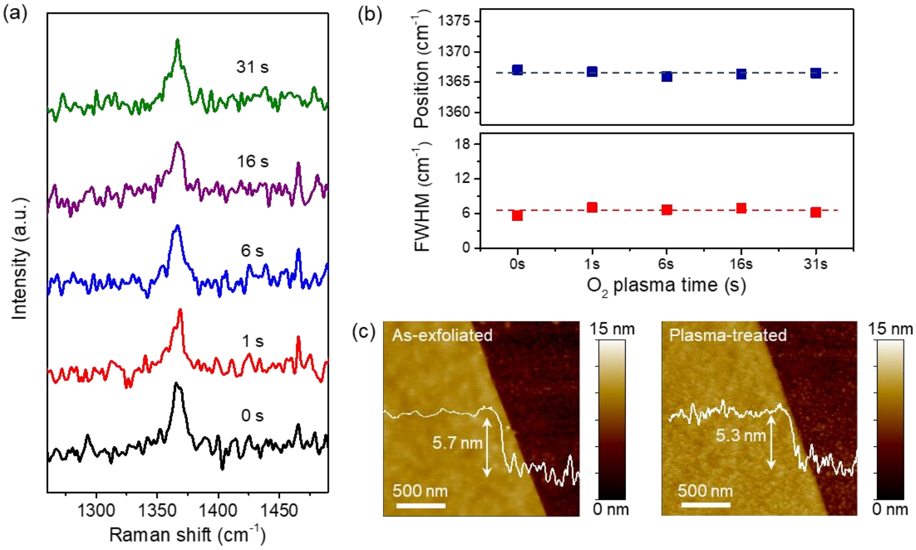

Figure 3.1.1 (a) Raman spectra of exfoliated hBNs before and after oxygen plasma time from 1s to 31s. (b) Variation of Raman peak position and full-width-at-half-maximum (FWHM) as a function of plasma time. (c) Topography of as-exfoliated and plasma-treated

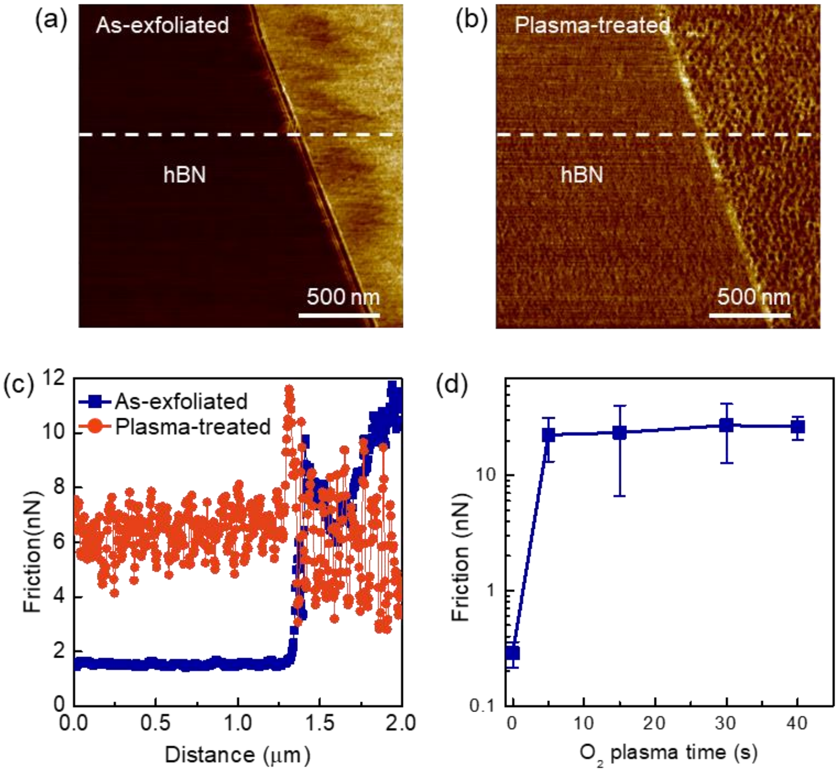

Figure 3.1.2 (a,b) Friction image of as-exfoliated and 14s plasma-treated hBN. (c) Profile of friction obtained along the white dashed line of (a,b), respectively. (d) Friction variation with oxygen plasma treatment time. The friction increases rapidly uo to 6s of plasma treatment time and saturated above 6s.

3.1.3.2 Photoluminescence from the midgap energy states

To investigate the defects-induced energy states, PL spectra of hBN after the oxygen plasma treatment were acquired using a laser of 325 nm wave length as shown in Figure 3.1.3(a). As the plasma treatment time increased, PL peaks emerged at 1.8, 2.3, 2.5 and 3.5 eV and gradually increased. To confirm the type of the defects responsible for the PL peaks, I performed the first-principles calculations based on the density functional theory (DFT). Figure 3.1.3(b) shows the structures of various defects, such as O substitution for nitrogen (O_N), B vacancy (V_B), B vacancy and O_N (V_BO_N), B vacancy saturated with two oxygen atoms (V_BO_2), and N vacancy (V_N) and their in-gap states calculated by using a hybrid functional HSE06. I listed possible transition energy values, which are corresponding to the PL peaks. The first PL peak at 1.8 eV is associated with transition energy between the in-gap state of O_N and the conduction band. The other three PL peaks at 2.3, 2.5 and 3.5 eV are comparable to the transition energies calculated from V_B, V_BO_N/V_N, and V_BO_2, respectively. Therefore, the emerged PL peaks in the plasma-treated hBN are ascribed to the transitions within the midgap energy states of the defects. In order to generate the more defect-induced energy states, I measured PL spectra with longer oxygen plasma treatment time up to 76s. As shown in the Figure 3.1.3(c), PL intensity originated from the defects increases and is saturated around 30 s. This indicates that, as the hBN is etched simultaneously, total number of defects is maintained. Therefore, it is estimated that the band gap is constant after plasma treatment of 30 s.

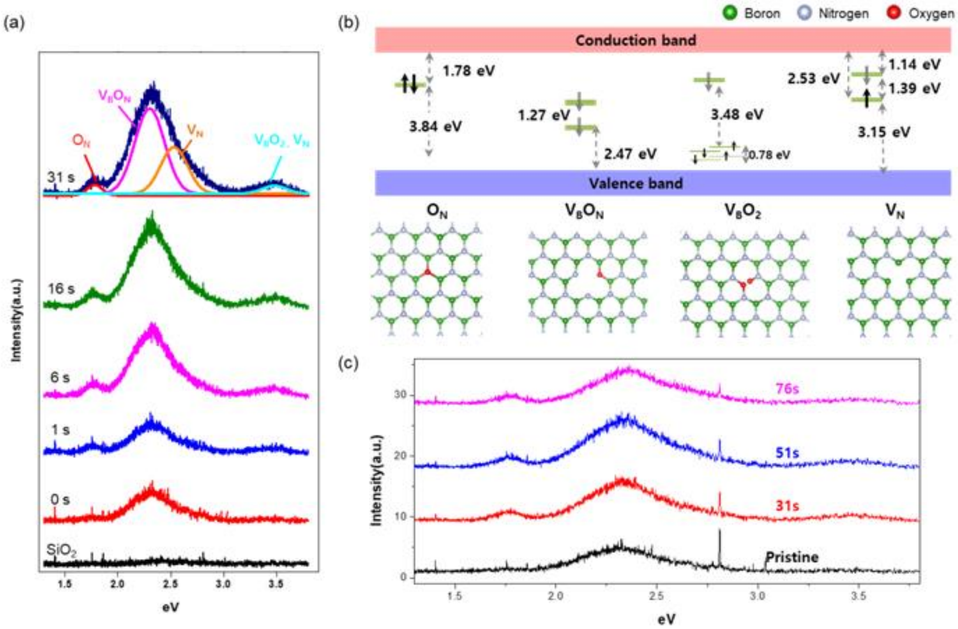

Figure 3.1.3 (a) Photoluminescence (PL) spectra of the hBNs before and after oxygen treatment time from 1s to 31s. The PL peaks increased with the plasma treatment time. (b) Top view of the five defect structures O_N, V_B, V_BO_N, V_BO_2 and V_N, and in-gap states calculated by using a hybrid functional HSE06. Black (gray) arrows indicate spin up and down at occupied (empty) states. (c) PL spectra of the plasma treated hBN for different time. The PL intensity originated from the defects increases and is saturated around 30 s.

PES was measured to investigate the surface chemical composition of the oxygen plasma-treated hBN at hν=750 eV. For the as-exfoliated hBN, figure 3.1.4(a) shows the main peak of B 1s and N 1s of core-level spectra that are located at 190.8 eV and 398 eV, respectively, which are in agreement with the previous reports of B-N bonding.(61-63) However, no O 1s peak was observed for the as-exfoliated hBN. After the oxygen plasma treatment of 14 s, the main peak intensities of B 1s and N 1s decreased dramatically along with the increased peak width as shown in Figure 3.1.4(b). Unless noted otherwise, all samples used for analyses were treated by oxygen plasma for 14 s. The PES spectra were deconvoluted by using Gaussian fitting to extract the component peaks. The component peaks at 191.4 and 192.5 eV of the B 1s and 399.5 and 400.6 eV of the N 1s correspond to the BN_xO_y, B-O, BN_xO_y and N-O bonds, spectrum consisting of three component peaks emerged at 531, 533 and 534 eV after plasma treatment of 14 s, which indicates that O-B-N complexes are generated.(64) From the PES results, it can be noted that the ionized oxygen breaks B-N bonds and induces various defects such as V_B, V_N and oxygen-related bonds in the plasma-treated hBN. Figure 3.1.5 shows the relative atomic ratio obtained by calculating the area of the PES peaks (the area of N is normalized to 1) before and after plasma treatments for 14 s. While the as-exfoliated hBN reveals boron-rich condition, the relative atomic ratio of boron decreased from 1.27 to 0.59 after plasma treatment. It means that boron is more susceptible to oxygen plasma compared to nitrogen. Although the previous theoretical studies have reported that the formation energy of V_B is higher than that of V_N (65, 66), V_B was found to be generated more than V_N from our experimental results. The dominant V_B can be explained by the threshold beam energies of boron and nitrogen. For the damage of hBN induced by energetic electron irradiation, the boron atom can be removed more easily due to its smaller threshold emission energy.(67, 68) It is important to note that the oxygen plasma process can generate dominant V_B type defect in hBN lattice. As a result, oxygen plasma treatment generates V_B more than V_N, resulting in nitrogen-rich condition in hBN. In order to more correct quantitative chemical analysis. I conducted EELS for hBN before and after oxygen plasma treatment. As shown in the Figure 3.1.6, amounts of B and N decreased after plasma treatment, meanwhile the oxygen was not detectable. Furthermore, because the defects in the plasma-treated hBN have complicated forms, such as V_B, V_BO_N/V_N, and V_BO_2, it is difficult to exactly identify the defect type by using quantitative analysis of EELS.

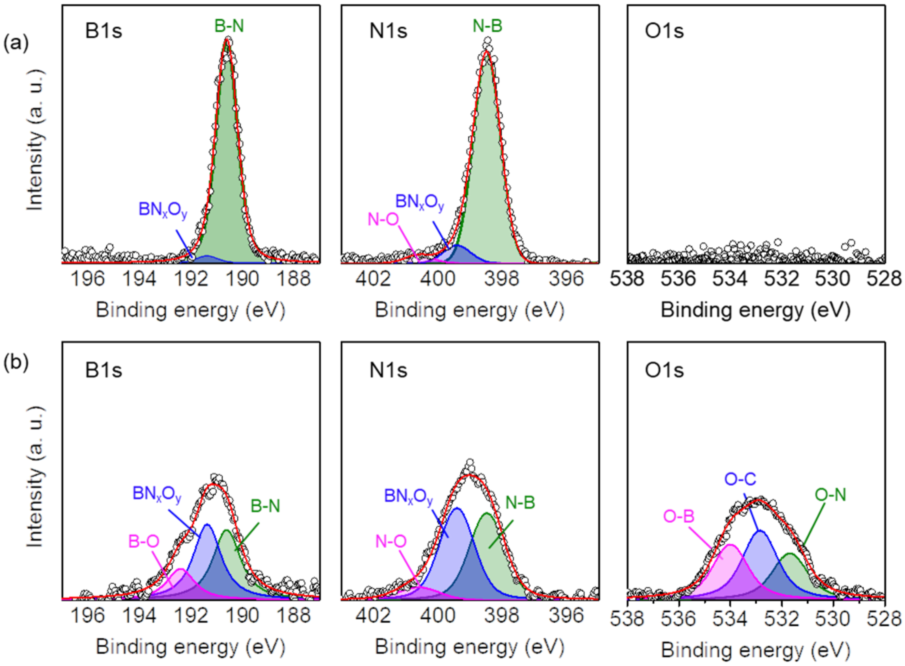

Figure 3.1.4 Comparison of PES results of (a) as-exfoliated and (b) plasma-treated hBNs. After the oxygen plasma treatment for 14 s, the B-N-O complex was generated corresponding to the defects calculated by using a hybrid functional HSE06.

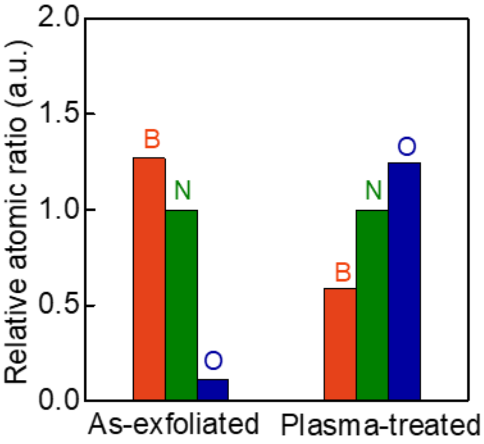

Figure 3.1.5 Relative atomic ratio of as-exfoliated and plasma-treated hBN. Atomic ration was calculated based on nitrogen. The boron relative atomic ratio of plasma-treated hBN decreased from 1.27 to 0.59. It means that boron is more easily removed by oxygen plasma than nitrogen

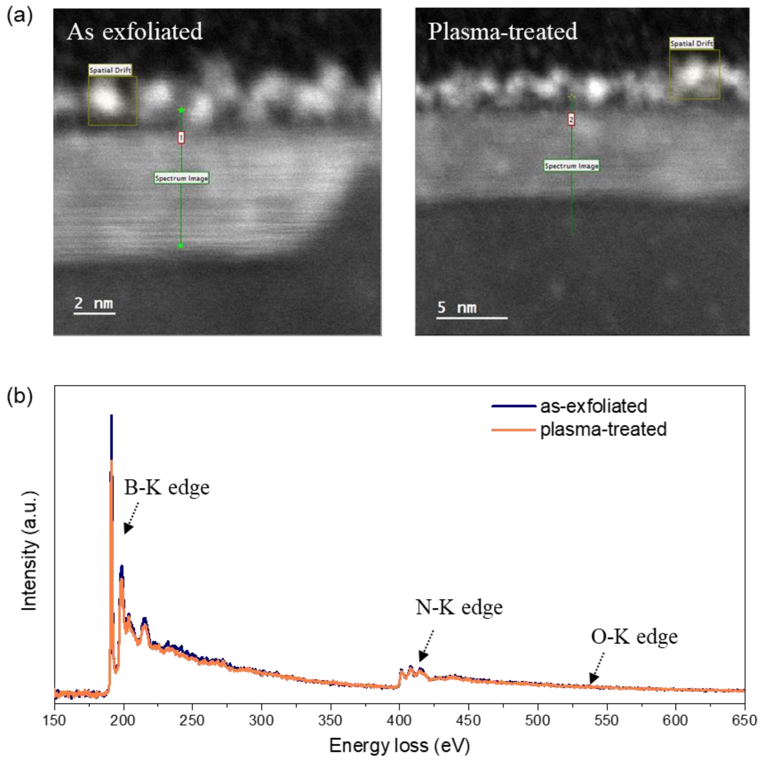

Figure 3.1.6. EELS analyses of the plasma-treated hBN. The Cs-STEM image (a) and EELS spectra (b) of the hBN before and after oxygen plasma. The blue and orange colored spectrums are as-exfoliated and plasma-treated of hBN, respectively.

3.1.3.3 Insulating properties and band structure

I measured the tunneling current through the plasma-treated hBN to verify the insulating property. The hBN was exfoliated onto an Au-coated SiO2 substrate for c-AFM measurement. Figure 3.1.7(a) shows the I-V curves measured through the as-exfoliated and plasma-treated hBN with the thickness of 5.7 and 5.4 nm, respectively. The threshold voltage for tunneling of the as-exfoliated hBN was 0.8 V/nm which is in agreement with previous reports (69), meanwhile the plasma-treated hBN showed a smaller threshold voltage of ~0.23 V/nm. Nevertheless, there is no recognizable change of threshold voltage regardless of the applied sweep voltage (Figure 3.1.8). The layered structure of plasma-treated hBN was investigated by using a cross-section TEM as shown in Figure 3.1.7(b,c). The generated defects were observed mainly in the topmost layers and inside of plasma-treated hBN. It is estimated that the defect paths in the plasma-treated hBN allow for the Poole-Frenkel tunneling at smaller bias(70). To measure the shift of work function, the surface potentials of the as-exfoliated and plasma-treated hBNs were measured by KPFM. Figure 3.1.9(a) and (b) shows the height and contact potential difference (CPD) maps of the as-exfoliated and plasma-treated hBNs, respectively. The CPD between the AFM tip and sample is given by

$$\boldsymbol{CPD = \frac{\emptyset_{tip} - \emptyset_{sample}}{e}}$$

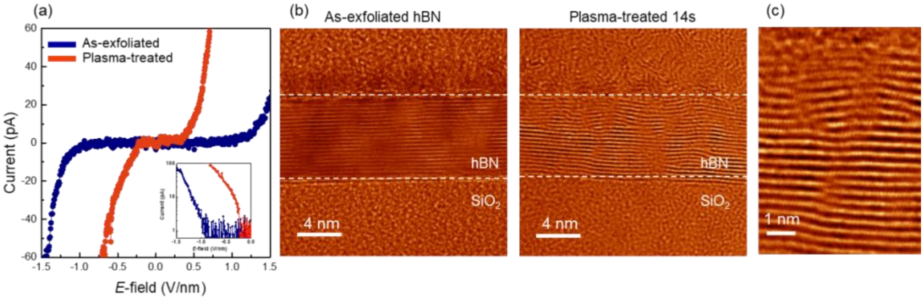

Figure 3.1.7 (a) Tunneling current of as-exfoliated and plasma-treated hBNs at varying tip bias (inset: logarithmic scale). (b) Cross-sectional TEM images of as-exfoliated and plasma-treated hBNs. (c) Magnified TEM images of plasma-treated hBN.

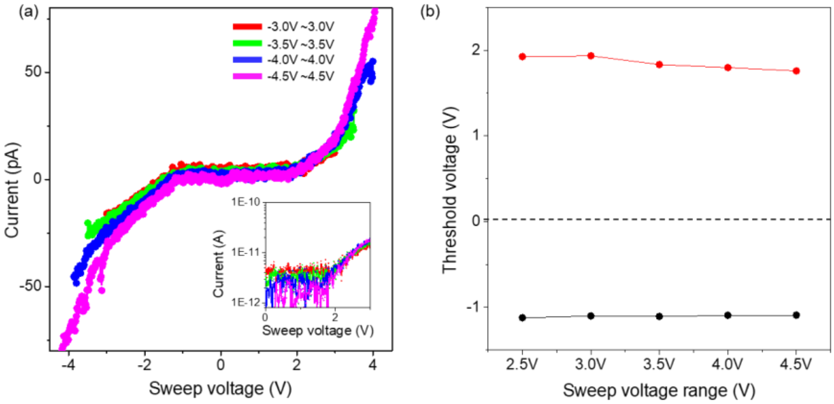

Figure 3.1.8 (a,b) Thresold voltage of plasma-treated hBN as a function of sweep voltage. Below the I/V conditions, oxygen plasma-treated hBN was not deformed by I-V spectroscopy, regardless of current detection

where $\emptyset_{tip}$, $\emptyset s_{ample}$, and e are the work functions of the Pt-coated tip and the hBN sample, and the elementary charge, respectively. The CPD of the as-exfoliated hBN shifted from 0.12 V to -0.31 V after the oxygen plasma treatment as shown in Figure 3.1.10. The work function of the Pt-coated tip was calibrated using a gold film (∅Au = 5.05 eV). As a result, the calculated work function of the plasma-treated hBN is 5.44 eV as shown in Figure 3.1.9(b). This indicates that the Fermi level of the plasma-treated hBN moves closer to its valence band. Figure 3.1.11(a) shows the spectra of the valence band maximum (VBM) and conduction band minimum (CBM) of the as-exfoliated and plasma-treated hBNs measured by the PES and NEXAFS, respectively. The PES spectra show that the energy difference between the Fermi level and VBM decreased from 2.5 to 1.7 eV after the plasma-treatment. It indicates that VBM of plasma-treated hBN upshifted toward the Fermi level, which agrees with the work function shift measured in Figure 3.1.11(b). In the B K-edge NEXAFS spectra (red line) of Figure 3.1.11(a), In the B K-edge NEXAFS spectra (red line) of Figure spectra show that the energy difference between the Fermi level and VBM decreased from 2.5 to 1.7 eV after the plasma-treatment. It indicates that VBM of plasma-treated hBN upshifted toward the Fermi level, which agrees with the work function shift measured in Figure 3.1.9(b). In the B K-edge NEXAFS spectra (red line) of Figure 3.1.11(a), π* peak was observed at ~193.7 eV, which is a characteristic feature of hBN. (71) After the oxygen plasma treatment, the intensity of the π* peak decreased significantly and downshifted by 0.4 eV. V. Therefore, the band gap of the hBN was reduced from 5.7 to 4.5 eV due to increased defect states as depicted in Figure 3.1.11(b). This is probably due to the increased bonding length in the disordered crystal structure of hBN after plasma treatment. Our electrical measurements show that the electrical properties of the hBN can be modulated by controlling the density of defects through the oxygen plasma treatment.

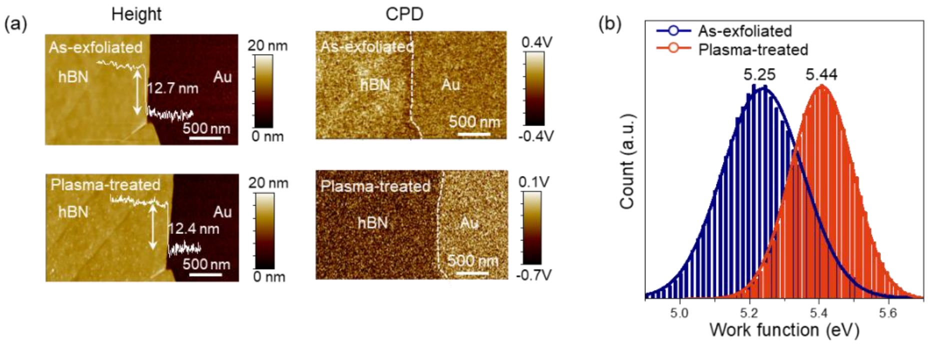

Figure 3.1.9(a) Thickness and contact potential difference (CPD) images before and after oxygen plasma. The dash line denotes the boundary between hBNs and Au substrate. (b) Work function variation of hBNs by oxygen plasma.

(a) As-exfoliated

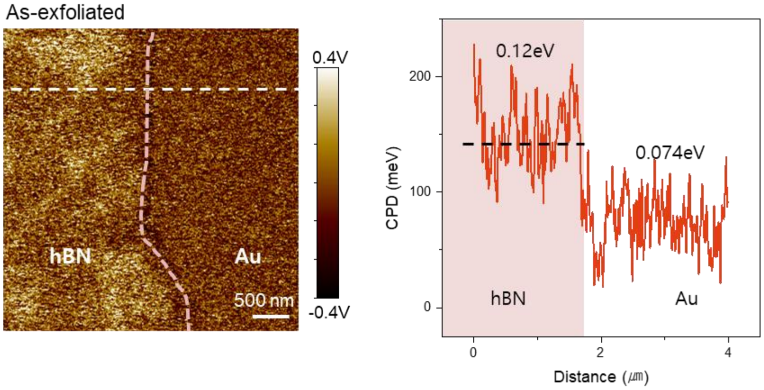

(b) Plasma-treated

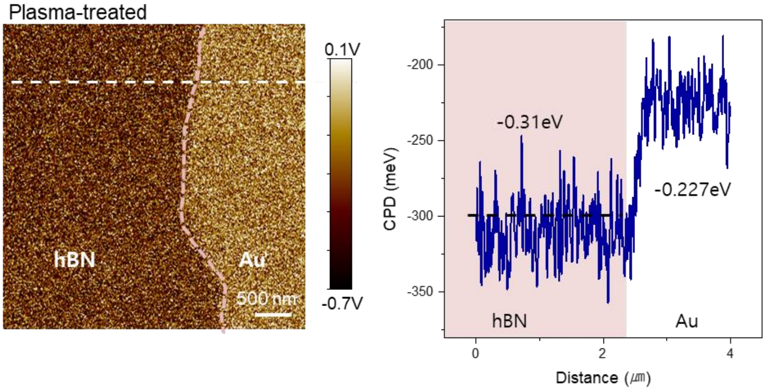

Figure 3.1.10.KPFM images and CPD of hBN flake before (a) and after (b) oxygen plasma. The CPD of the plasma-treated hBN demonstrates a remarkable reduction by ~ -0.31 eV. This shows the shift of the Fermi level of plasma-treated hBN.

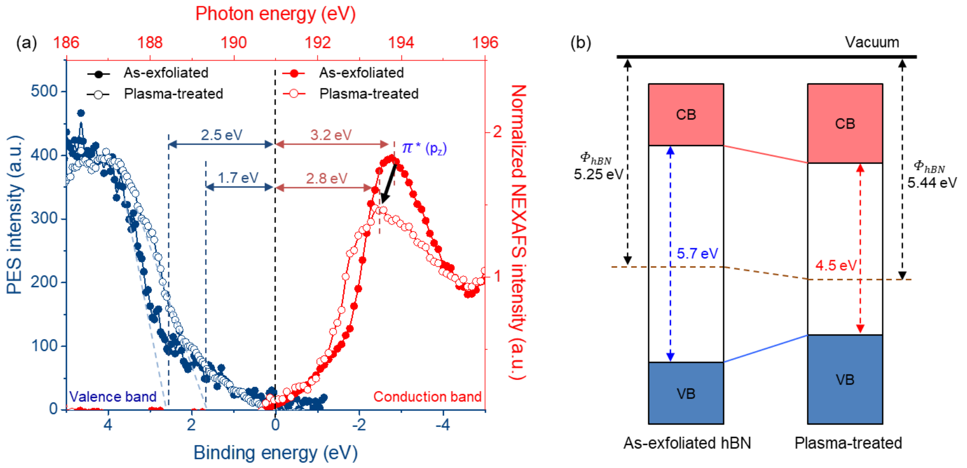

Figure 3.1.11 (a) PES and NEXAFS spectra of as-exfoliated and plasma-treated hBNs. Blue and red lines indicate the VBM and CBM of as-exfoliated and plasma-treated hBNs, respectively. Black arrow shows the shift of CBM. (b) Schematic of bandgap tuning by oxygen plasma of hBNs.

3.1.4 Conclusions

In this study, I demonstrated that the electrical properties were significantly modulated by various defects on the surface through the inside of hBN induced by the oxygen plasma treatment. Although the hBN is a representative insulator with a large bandgap, the oxygen plasma process modulates the electrical property of hBN by easily generated the defects and then the bandgap of hBN was reduced from 5.7 eV to 4.5 eV. Raman spectroscopy showed the enhanced PL from specific defects states after certain duration of oxygen plasma, which indicates the increased density of defects. The DFT calculation elucidated that the types of oxygen-related defects are in good agreement with the PL data. Moreover, the PES analysis revealed that the defect types can be controlled by oxygen plasma via the generation of specific defects such as V_B. Our results showed the optical and electrical properties of hBN can be significantly modulated by the oxygen plasma process, and it is an important factor to be considered in the manufacturing process of robust 2D electronic devices using hBN in the future.

* This chapter has been published in a journal. Manuscript is reproduced with permission from Na et al., *Adv. Func. Mater.* (2022) 2207351

3.2. Conducive filament contacts for van der Waals hetero-structure devices

3.2.1 Introduction

Devices using two-dimensional materials are attracting attention as next-generation materials because of their high carrier mobility and improved short-channel effect.(25-27) However, 2D materials occurs in unintentional doping or degradation by polymer residues during fabrication process and active species in ambient atmosphere.(28) A clean channel layer in 2D devices can achieve high-performance, stable devices. Among the many passivation materials for 2D-based device, hexagonal boron nitride (hBN) of 2D insulator is an ideal material, as it has impermeability to water and oxygen, good thermal dissipation and boosting electrical performance of active layer.(29, 30) Accordingly, a 2D stacking technology that can construct the hBN-based van der Waals (vdWs) hetrostructure has been developed, and the vdW heterostructure which can be integrated vertically has a high potential for application in nano-device.(31-34)

As connection between metal electrode and embedded channel layer is essential in passivated vdW heterostructure, various contact methods have been proposed.

Edge contact is a method of contacting only the side edge of a metal electrode.(37, 38, 72) Edge contact based on graphene channel was reported for the first time, and it was developed as a hybrid contact in which the vdWs and edge contacts based on graphene electrode with transition metal dichacogenide (TMD) channel are combined.(24, 39) Moreover, the edge contact with TMD channel has been reported, but it has high contact resistance (R_c) due to oxidation on terminated edge during etching.(40-42) The edge contact technique still has many issues to solve such as challenging fabrication process, high R_c due to the small contact area and damage to the lower substrate via etching process. Another method is fluorinated graphene via contact using graphene etch stop (GES) technique with XeF_2 gas, as described in our previous report.(43) Although this technology was a first demonstration of 3D integration using 2D via contact, it is possible with only graphene rather than other 2D materials. Recently, transferred via contact, metal-predeposited hBN was transferred onto a TMD, was demonstrated.(44) The technique with vdWs contact can suppress the Fermi-level pinning effect and exhibited high hole mobility and low contact resistance through WSe_2 FET. However, the transfer method is not easy to align concisely when implementing the nano-device and the process was carried out in a glove box to prevent oxidation of the metal surface during transfer process. Therefore, a new approach on contact method in passivated vdW heterotucture is required.

Here, I introduce the new contact method with irreversible conductive filament (ICF) in defective hBN using repeated forming processes to connect metal and embedded 2D channel layer such as not only graphene but also TMD. In memristor structure, diffusion of metal ions in an insulator results in the formation of conductive filaments, when a voltage is applied. These conductive filaments are reversible due to reset process with reverse voltage, which can dissolve the metal filament and return the device to off state.

3.2.2 Experimental procedure

Device preparation: Mechanical exfoliation of a bulk crystal onto a 285nm SiO_2/Si substrate produced all flakes. I used atomic force microscopy to determine the thickness of the exfoliated sheet (AFM).The quality of the each sheets were investigated using Raman spectroscopy. The heterostructure were fabricated by stacking top hBN, graphene (or MoS_2), and bottom hBN via the pick-up transfer technique using a polydimethylsiloxane (PDMS) stamp coated with polycarbonate (PC) film.(32) The stacked heterostructure was transferred to a SiO2/Si substrate after the PC film was released from the PDMS at temperatures over 180℃. After transfer of the heterostructure, the PC carrier film was dissolved in chloroform overnight. To fabricate metal electrodes, I designed the electrodes with e-beam lithography deposited metals (Cr/Pd/Au (1/30/40nm) and Ag/Au (30/30nm)) via e-beam evaporation under ultrahigh vacuum condition of ~10^{-7} Torr. For generating defects, oxygen plasma treatments with a reactive ion etch (RIE) mode was carried out on the hBN using customized plasma equipment (FemtoScience, CUTE). The treatment parameters are as follows: RIE power (100 W), pressure (10^{-1} Torr), O_2 flow rate (20 sccm), frequency (100 kHz), and treatment time (30s).

Electrical measurement: Semiconductor parameter analyzers were used to do all electrical measurements (Keithley 4200A-SCS) at room temperature under ultralow vacuum of 10^{-2} Torr due to stable measurement. The heavily doped Si substrate serves as the global back-gate. The back-gate voltage (V_{BG}) was applied to modulate the electrical potential of the channel layer such as graphene and MoS_2.

3.2.3 Results and discussions

3.2.3.1 Formation of conductive filaments in hexagonal boron nitride

To form ICF, I generated a defect paths in hBN through which metal can migrate easily using oxygen (O_2) plasma treatment, as reported previous report. (73) When hBN is treated with O_2 plasma, defective paths are generated in the topmost layer and inside of hBN. As the paths can serve as favorable metal ion migration paths, conductive filament can easily diffuse through defective paths in hBN. Therefore, conductive filaments can be generated irreversibly by several electrical forming processes, and a via contact based on ICF can be constructed that can connect to a channel and metal in a hBN-passivated heterostructure (see Figure 3.2.1).

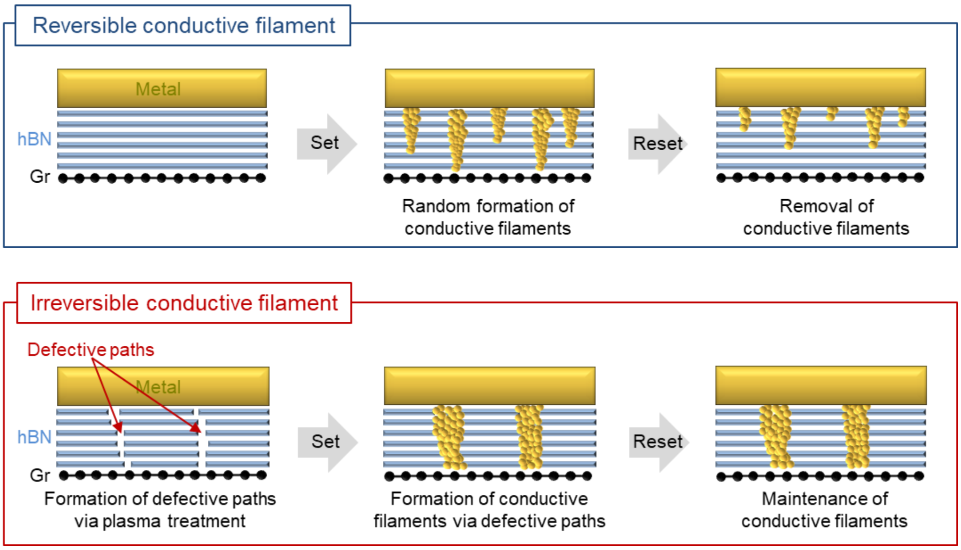

Figure 3.2.112. Mechanism of reversible and irreversible conductive filament formation in a vdWs heterostructure of hBN and graphene layer. Schematic of formation processes for reversible and irreversible conductive filament by electrical switching processes. When the hBN is pristine, conductive filament in hBN by electrical set process is reversible. When the hBN has defective path using plasma treatment, conductive filament is irreversible.

To demonstrate ICF contact device in figure 3.2.2 a, b, I fabricated a heterostructure of graphene FET encapsulated by hBN. The heterostructure was stacked with hBN1/Graphene/hBN2 structure on SiO_2 (285nm)/Si using a dry pick-up transfer technique.(32) (Figure 3.2.3,) Thickness of each stacked graphene and hBN is about 0.3~1nm and 3~6nm by measuring atomic force microscopy. (Figure 3.2.4) In the heterostructure, the half of the graphene was covered by the top hBN (hBN1), in order to fabricate two types electrode for ICF contact (CF1 and CF2) and conventional top contact (G1 and G2) in divided regions by hBN1. (region 1: hBN1/Gr/hBN2, region2 : Gr/hBN2 region) The region1 (hBN1/Gr/hBN2) patterned by e-beam lithography was exposed to O_2 plasma, generating defects in hBN1 for ICF contact. Raman spectra of the plasma treated regions showed no peak changes of graphene, indicating that the embedded graphene did not damage by the plasma treatment. (Figure 3.2.5) Then, 2nd e-beam lithography was carried out for additional metal leads in region2 (Gr/hBN2). Following direct deposition of Cr/Pd/Au metal by e-beam evaporation formed metal leads on hBN1 and Gr. In general, silver (Ag) ion is widely used in conductive filaments for memristive devices based on ion diffusion or oxygen vacancy. Since Ag has not only high mobility and low thermodynamic stability but also poor interaction with graphene, conductive filament of Ag can be easily rupture by reverse voltage for reset process. (74) So, I chose palladium (Pd) as ICF contact metal as it has low mobility and high thermodynamic stability. (75)

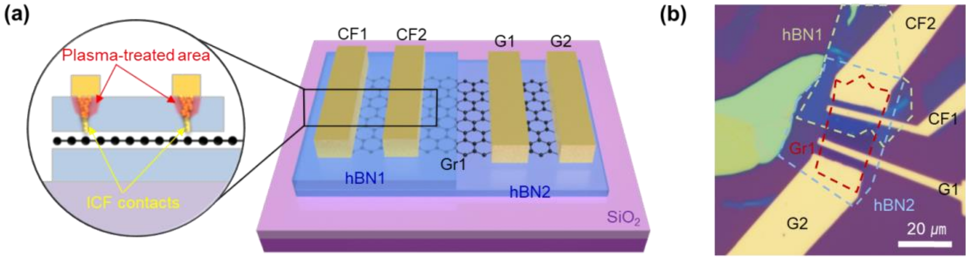

Figure 3.2.2. Device geometry of hBN-encapsulated graphene FET with irreversible conductive filament contact and conductive filament formation in the hBN using electrical set process. (a) Schematic of the a vdW heterostructure of embedded graphene FET with ICF contact

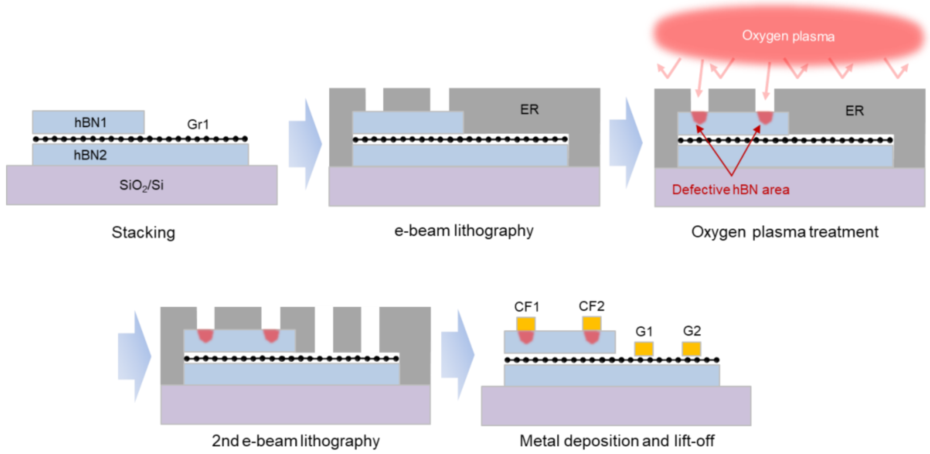

Figure 3.2.3. Fabrication process of hBN-encapsulated graphene FET with ICF contact. Schematics of fabrication processes of the embedded graphene FET with ICF contact. A series of schematics, representing each fabrication steps of stacking, lithography, oxygen plasma treatment, 2nd e-beam lithography and metal deposition.

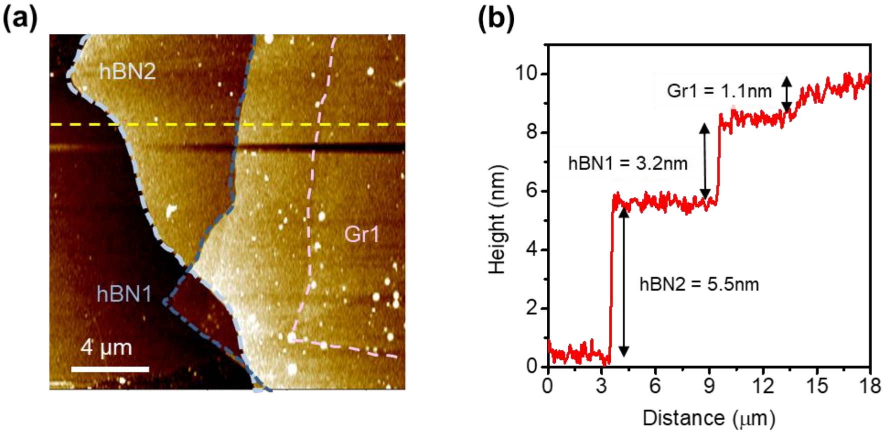

Figure 3.2.4. AFM data of vdW heterostructure of hBN1/Gr/hBN2 for conductive filament the device. (a) AFM image of the heterostructure. The dotted yellow lines are AFM measured region. (b) AFM topography profile of the heterostructure.

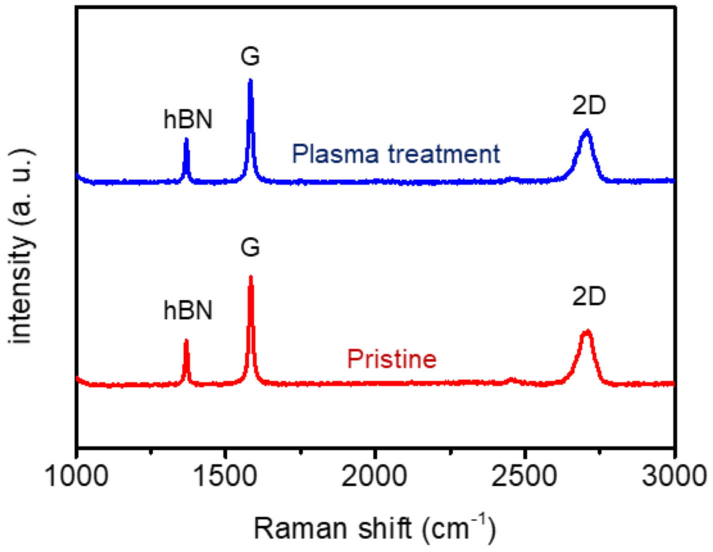

Figure 3.2.5. Raman spectra of vdW heterostructure of hBN1/Gr/hBN2 before and after oxygen plasma treatment for irreversible conductive filament contact. There is no change in Raman peaks, indicating that hBN-encapsulated graphene wasn't damaged by O_2 plasma.

3.2.3.2 Conductive filament contacts for graphene and MoS_2 devices

I first attempted to understand defect effect in hBN on forming the ICF of the device. Each G and CF electrodes are used as electrodes to apply bias voltage and ground, and gate voltage is applied by Si back gate to accumulate electrons in graphene channel. Between the devices depending on defect formation by O_2 plasma treatment, Figure 3.2.6 a and b show a noticeable difference in current-voltage (I-V) curves swept repeatedly in negative voltage (that is set process). The devices without plasma treatment exhibited no change in the shape of I-V curve ($I_{G1\text{-}CF1}$-$V_{G1\text{-}CF1}$), which maintained in tunneling behavior even after repeated set process – the tunneling current was slightly increased after several sweeps.

However, dramatic curve change was observed in the device with plasma treatment after several set process. As the number of sweeping negative voltage increases, the shape of I-V curve ($I_{G1\text{-}CF1}$-$V_{G1\text{-}CF1}$) gradually changes from the tunneling behavior to an ohmic behavior. In figure 3.2.6 (e), shape of the I-V curve ($I_{G1\text{-}CF1}$-$V_{G1\text{-}CF1}$) before the forming process and after the 50 repetitions of forming process was measured markedly different, which means that O_2 plasma treatment for defect generation is key requirement for formation of ICF.

.

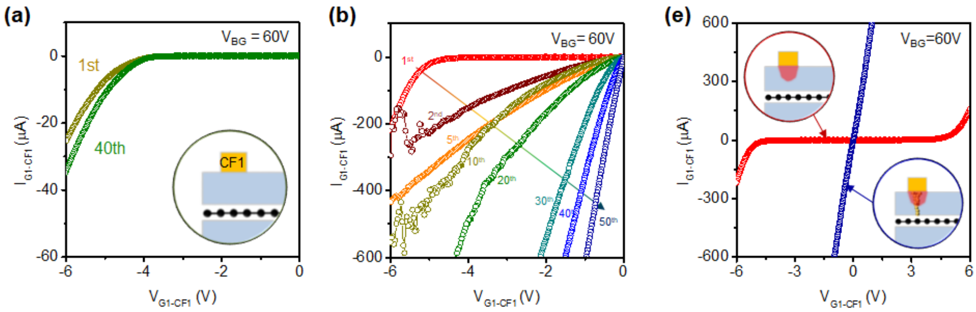

Figure 3.2.6. (a) Output curve (I_{G1}-CF1-V_{G1}-CF1) of device at fixed VBG of 60V without plasma treatment. The 1st sweep curve (dark yellow curve) is comparable to 40th sweep curve (green curve) due to not forming conductive filament. (b) Output curve ($I_{G1\text{-}CF1}$-$V_{G1\text{-}CF1}$) of the device with multiple sweeps at fixed V_{BG} of 60V to form conductive filament. As the number of sweeps increases, the output curve shows more conductive. (c) Output curve ($I_{G1\text{-}CF1}$-$V_{G1\text{-}CF1}$) at fixed V_{BG} of 60V before (red curve) and after (blue curve) forming conductive filament. Before forming the conductive filament, the output curve shows non-linear tunneling behavior. After the conductive filament is formed, the output curve shows a linear ohmic behavior

After forming the conductive filament in hBN, I tested that our conductive filament is irreversible through additional 50 repetition of sweeping forward and reverse bias of switching process in memristors. As shown in figure 3.2.7(a), little change in I-V curve ($I_{G1\text{-}CF1}$-$V_{G1\text{-}CF1}$) was observed, indicating that conductive filament is irreversible. Figure 3.2.7(b) shows the electrical transport through a graphene channel with CF and G electrode. The transfer curve ($I_{G1\text{-}CF1}$-V_{BG}) was V-shaped with no hysteresis and charge neutrality point shifted to zero voltage, which is similar to performance of hBN-encapsulated graphene. The gate current is about 10^{-11}A, indicating that the current flows through only conductive filament without leakage below substrate. As shown in Figure 3.2.7(c), the output curves ($I_{G1\text{-}CF1}$-$V_{G1\text{-}CF1}$) of the Gr FET with CF and G contact showed a linear behavior, indicating perfect connection between metal and graphene through conductive filament in hBN. By additionally forming to CF2 electrode via same set process as CF1 electrode, I explored the performance of the ICF contacts using hBN-encapsulated graphene FET. (Figure 3.2.8)

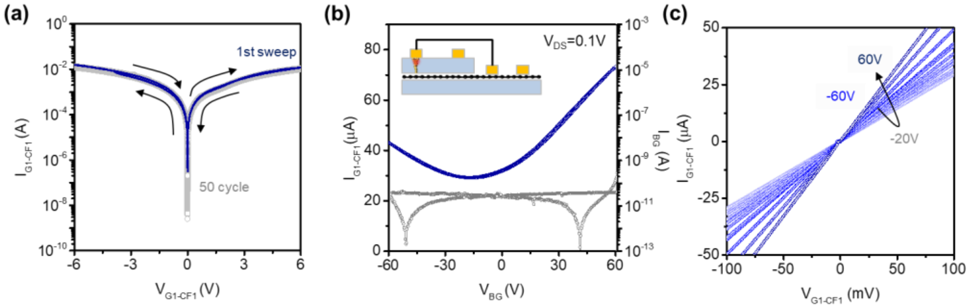

Figure 3.2.7 Electrical characteristic of the graphene FET with ICF contact after forming conductive filament. (a) Output curve (I_{G1}-CF1-V_{G1}-CF1) of repeated 50 cycle after forming process. After forming process, output curve during 50 cycles is nearly uniform. (b) Transfer curve (I_{G1-CF1}-V_{BG}) of the device at fixed V_{DS} of 0.1V (c) Output curve (I_{G1-CF1}-V_{G1-CF1}) of the device varying with V_{BG}

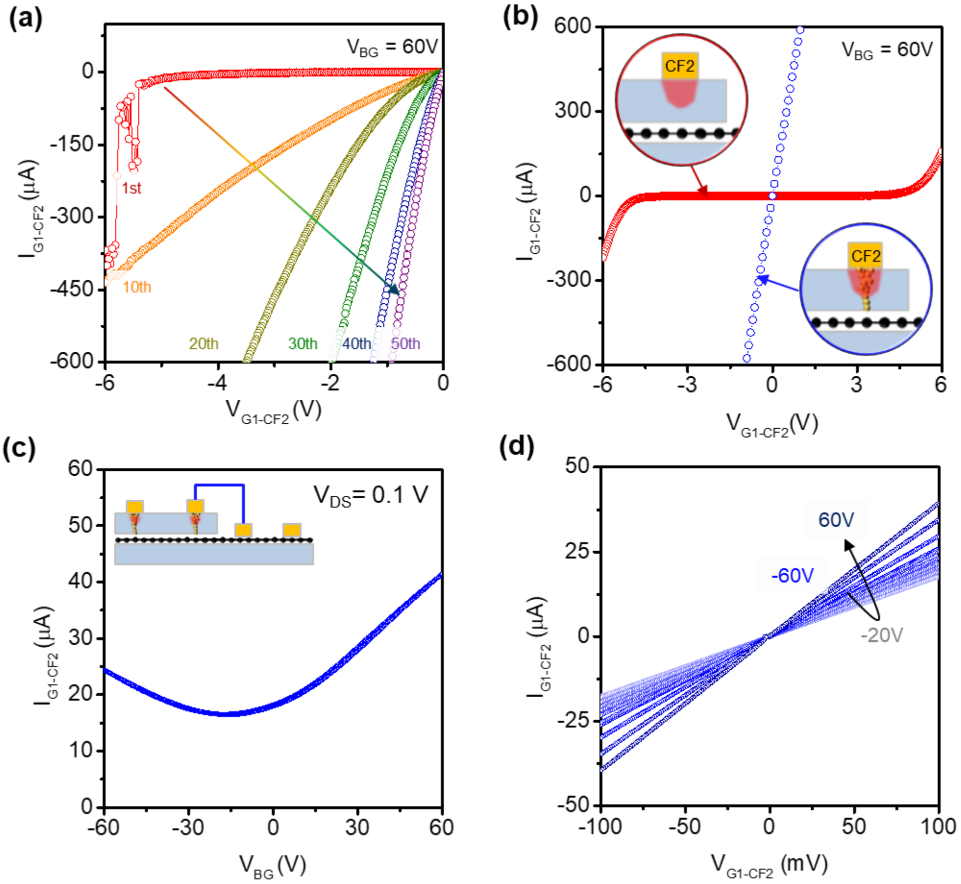

Figure 3.2.8 Conductive filament formation in hBN of embedded graphene device with CF2 electrode using electric field (a) Output curve (IG1-CF2-VG1-CF2) with multiple sweeps at fixed VBG of 60V to form conductive filament. As the number of sweeps increases, the output curve shows more conductive. (b) Output curve ($I_{G1\text{-}CF2}$-$V_{G1\text{-}CF2}$) at fixed V_{BG} of 60V before (red curve) and after (blue curve) forming conductive filament. (c) Transfer curve ($I_{G1\text{-}CF2}$-V_{BG}) of the device at fixed V_{DS} of 0.1V (h) Output curve ($I_{G1\text{-}CF2}$-$V_{G1\text{-}CF2}$) of the device varying with V_{BG}

To verify universality of our contact with various channel, I fabricated another FET with MoS_2 channel of n-type 2D semiconductor with the ICF contact of Ag metal. Although Ag has not good to form conductive filament due to high mobility and low thermodynamic stability, it was reported that Ag-MoS_2 contact exhibited ohmic behavior with high current injection efficiency due to low work function of the Ag. (76) Figure 3.2.9(a) shows schematics and optical image of device structure of the hBN-encapsulated MoS_2 FET with ICF contact. Similar to electrical forming process of ICF contact based on graphene FET, I-V curve ($I_{M1\text{-}CF1}$-$V_{M1\text{-}CF1}$) of MoS_2 FET changes to gradually conductive as the number of swept voltage increases, indicating that the ICF contact is also easily formed in MoS_2 channel as shown Figure 3.2.9(b). Additionally, I compared in performance on MoS_2 FET using ICF contact (CF1-CF2) and top contact (M1-M2). The transport of both MoS_2 FETs using ICF and top contact showed n-type semiconducting behaviors observing at conventional MoS_2 FET in Figure 3.2.9(c). The MoS_2 FET with ICF contact showed a field effect mobility of 1.11cm^2/Vs with excellent on/off ratio of 10^7 and output curve of the device has schottky contact in figure 3.2.9(d). Top contacted-MoS_2 FET exhibited comparable performance of on-current and field effect mobility 1.57cm^2/Vs to that of ICF contacted device. I used the Y-function method to obtain the contact resistance(Rc) of the ICF contact device. The contact resistance is 446 kΩμm.(77) The hBN-encapsulated ICF contact device has a lower threshold voltage because the top contact is n-doped as a result of adsorbent material. This is similar to the top contact device (491 km).(78, 79)

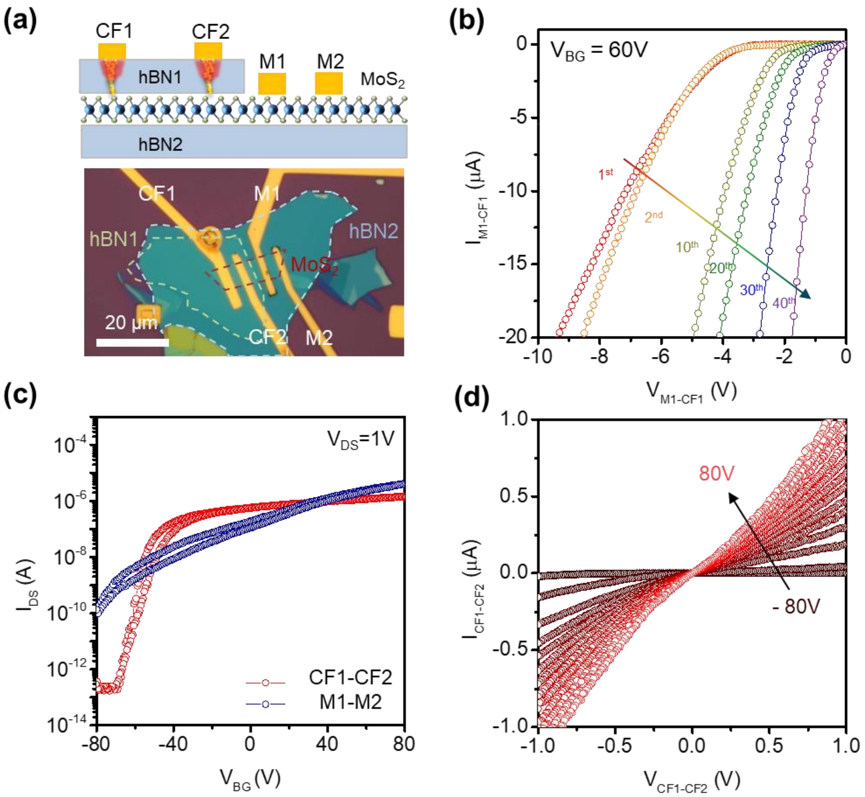

Figure 3.2.9. n-type semiconducting transported MoS2 channel with ICF contact (a) Schematic of the a vdW heterostructure of embedded MoS2 FET with ICF contact and optical image of a corresponding heterostructure of the fabricated device. (b) Output curve ($I_{M1\text{-}CF1}$-$V_{M1\text{-}CF1}$) of the device with multiple sweeps at fixed V_{BG} of 60V to form conductive filament. (c) Transfer curve ($I_{M1\text{-}CF1}$-V_{BG}) at fixed V_{DS} of 1V. Transfer curve show n-type semiconducting transport behavior comparable to conventional MoS_2 FET. (d) Output curve ($I_{CF1\text{-}CF2}$-$V_{CF1\text{-}CF}$) varying with V_{BG}. The output curve shows a non-linear ohmic behavior, indicating ICF contact of MoS_2 channel is schottky contact.

3.2.3.3 Reliability of conductive filament contacts

Figure 3.2.10(a and b) plots electrical properties of the graphene device with ICF contacts. Transfer curve ($J_{CF1-CF2}$-$V_{CF1-CF2}$) showed the characteristic of graphene transport which is similar to that of graphene FET using ICF and G electrode in figure 3.2.10 (b). It means that device resistance is mainly contributed to channel resistance rather than contact resistance. Furthermore, no hysteresis is presented in hBN-encapsulated graphene devices because of the clean interface between graphene and hBN and free charge trap of hBN. (35, 80) In figure 3.2.10(b) The output curves (JCF1-CF2-VCF1-CF2) of the graphene FET with ICF contacts exhibited linear behavior at a wide range of gates, indicating the Ohmic contact at ICF contact.. As shown in figure 3.2.10.(c), the current density of graphene FETs with Pd-ICF contacts is significantly superior to than that with Ag electrodes. It is attribute to strong interaction between Pd and graphene, arising to small sensitive to the atomistic configuration of contact resistance.(81) In addition, the Pd-graphene contact has a lower contact resistance than other metals in case of top contact. (82)

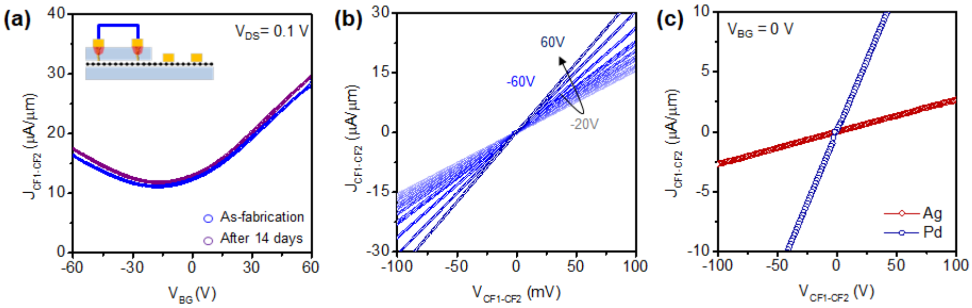

Figure 3.2.10. (d) Transfer curve (JCF1-CF2-VG2) of the device at fixed VDS of 0.1V at as-fabrication and after 14 days. Transfer curve show V-shaped curve comparable to conventional graphene FET and the conductive filament is maintained over the time pass. (e) Output curve ($J_{CF1-CF2}$-$V_{CF1-CF2}$) varying with $V_{BG.}$ The output curve shows a linear ohmic behavior, indicating ICF contact is ohmic contact. (f) Output curve ($J_{CF1-CF2}$-$V_{CF1-CF2}$) of the device with ICF contact of Ag (dark red curve) and Pd metal (dark blue curve). The current density of Pd-ICF contact is superior to that with Ag-ICF contact

3.2.4 Conclusions

I demonstrate new contact way using irreversible conductive filament for connecting metal and embedded active channel of 2D materials. Contrary to reversible conductive filament in pristine 2D materials, our work reveals defects by O_2 plasma treatment are prerequisite for forming irreversible conductive filament because defects are favorable metal diffusion path. Based on the fact, the fabricated device using ICF contacts has compatible performance of that using conventional top contact. In addition, I believe that ICF contact performance could be improved with further works such as various engineering. So, this work reports useful contact, which has high potential for idealized 2D electronics device.

.

Chapter 4. Summary

In this thesis, I introduce modulation of electrical-optical on defective hBN and new strategy for contact method using conductive filaments. The defects are useful for many fields such as quantum nanophotonic, memory device and neuromorphic. I summarize defect engineering of hBN for electronic applications.

- I demonstrated modulation of hBN properties, such as optical and electrical, by defects generated using mild oxygen plasma. This method can generate various defects, such as V_B , V_BO_N , O_N, , , V_BO_2 and V_N, leading to emerged photoluminescence (PL) mainly at around 1.8 ~ 3.5 eV visible range. Also, band gap of plasma-treated hBN is changed from 5.7 to 4.5 eV. Furthermore, as shown in the PES results, oxygen plasma can generate specific defects such as boron vacancies.

-Novel contact method: I demonstrated fabrication technique of the ICFs in the encapsulated-hBN devices to electrically connect the channels inside the device. By treat the hBN with oxygen plasma, the ICF with high stability and low resistance can be fabricated by metal ions and vacancies present in the defect path formed in hBN. My results provide the intrinsic properties of hBN can be dramatically changed via oxygen plasma treatment leading to control of the type and density of defects systemically and new contact method for 2D vdW heterostructure device. In the future, these results will play an important role in the application of electro-optical devices using hBN.

References

1.Novoselov KS, Geim AK, Morozov SV, Jiang D, Zhang Y, Dubonos SV, et al. Electric field effect in atomically thin carbon films. Science. 2004;306(5696):666-9.

2.Novoselov KS, Jiang D, Schedin F, Booth TJ, Khotkevich VV, Morozov SV, et al. Two-dimensional atomic crystals. Proc Natl Acad Sci U S A. 2005;102(30):10451-3.

3.Schwierz F. Graphene transistors. Nat Nanotechnol. 2010;5(7):487-96.

4.Pacile D, Papagno M, Rodriguez AF, Grioni M, Papagno L, Girit CO, et al. Near-edge x-ray absorption fine-structure investigation of graphene. Phys Rev Lett. 2008;101(6):066806.

5.Wang QH, Kalantar-Zadeh K, Kis A, Coleman JN, Strano MS. Electronics and optoelectronics of two-dimensional transition metal dichalcogenides. Nat Nanotechnol. 2012;7(11):699-712.

6.Daniel Rhodes1, Sang Hoon Chae1,3, Rebeca Ribeiro-Palau2 and James Hone. Disorder in van der Waals heterostructures
of 2D materials. Nature Materials. 2019;18:541–9.

7.Kubota Y, Watanabe K, Tsuda O, Taniguchi T. Deep ultraviolet light-emitting hexagonal boron nitride synthesized at atmospheric pressure. Science. 2007;317(5840):932-4.

8.Y. M. Shi CH, X. T. Jia, K. K. Kim, A. Reina,, M. Hofmann ALH, K. Zhang, H. N. Li, Z. Y. Juang,, M. S. Dresselhaus LJLaJK. High thermal conductivity of suspended few-layer hexagonal boron nitride sheets. Nano Lett. 2010;10
4134–9.

9.Dean CR, Young AF, Meric I, Lee C, Wang L, Sorgenfrei S, et al. Boron nitride substrates for high-quality graphene electronics. Nature Nanotechnology. 2010;5(10):722-6.

10.Watanabe K, Taniguchi T, Kanda H. Direct-bandgap properties and evidence for ultraviolet lasing of hexagonal boron nitride single crystal. Nat Mater. 2004;3(6):404-9.

11.Golberg D, Bando Y, Huang Y, Terao T, Mitome M, Tang C, et al. Boron nitride nanotubes and nanosheets. ACS Nano. 2010;4(6):2979-93.

12.Britnell L, Gorbachev RV, Jalil R, Belle BD, Schedin F, Mishchenko A, et al. Field-effect tunneling transistor based on vertical graphene heterostructures. Science. 2012;335(6071):947-50.

13.Roy T, Tosun M, Kang JS, Sachid AB, Desai SB, Hettick M, et al. Field-effect transistors built from all two-dimensional material components. ACS Nano. 2014;8(6):6259-64.

14.Tae Hoon Lee† KKO, Gwangwoo Kim, Hyo Ju Park#, Declan Scullion, Leo ShawOrcid, Myung-Gil Kim, Xiaodan Gu, Won-Gyu Bae, Elton J. G. Santos, Zonghoon Lee Orcid, Hyeon Suk Shin@Orcid, Yoshio Nishi*†, and Zhenan Bao*. Chemical Vapor-Deposited Hexagonal Boron Nitride as a Scalable Template for High-Performance Organic Field-Effect Transistors. Chem Mat. 2017; 29, 5: 2341–7.

15.Dean CR, Young AF, Meric I, Lee C, Wang L, Sorgenfrei S, et al. Boron nitride substrates for high-quality graphene electronics. Nat Nanotechnol. 2010;5(10):722-6.

16.Jang AR, Hong S, Hyun C, Yoon SI, Kim G, Jeong HY, et al. Wafer-Scale and Wrinkle-Free Epitaxial Growth of Single-Orientated Multilayer Hexagonal Boron Nitride on Sapphire. Nano Lett. 2016;16(5):3360-6.

17.Kretinin AV, Cao Y, Tu JS, Yu GL, Jalil R, Novoselov KS, et al. Electronic properties of graphene encapsulated with different two-dimensional atomic crystals. Nano Lett. 2014;14(6):3270-6.

18.Tran TT, Bray K, Ford MJ, Toth M, Aharonovich I. Quantum emission from hexagonal boron nitride monolayers. Nat Nanotechnol. 2016;11(1):37-41.

19.Wu X, Ge R, Chen PA, Chou H, Zhang Z, Zhang Y, et al. Thinnest Nonvolatile Memory Based on Monolayer h-BN. Adv Mater. 2019;31(15):e1806790.

20.Chhowalla M, Shin HS, Eda G, Li LJ, Loh KP, Zhang H. The chemistry of two-dimensional layered transition metal dichalcogenide nanosheets. Nat Chem. 2013;5(4):263-75.

21.Yoon Y, Ganapathi K, Salahuddin S. How good can monolayer MoS(2) transistors be? Nano Lett. 2011;11(9):3768-73.

22.Radisavljevic B, Radenovic A, Brivio J, Giacometti V, Kis A. Single-layer MoS2 transistors. Nature Nanotechnology. 2011;6(3):147-50.

23.Splendiani A, Sun L, Zhang Y, Li T, Kim J, Chim CY, et al. Emerging photoluminescence in monolayer MoS2. Nano Lett. 2010;10(4):1271-5.

24.Wang L, Meric I, Huang PY, Gao Q, Gao Y, Tran H, et al. One-Dimensional Electrical Contact to a Two-Dimensional Material. Science. 2013;342(6158):614-7.

25.Liu Y, Duan X, Shin HJ, Park S, Huang Y, Duan X. Promises and prospects of two-dimensional transistors. Nature. 2021;591(7848):43-53.

26.Desai Sujay B, Madhvapathy Surabhi R, Sachid Angada B, Llinas Juan P, Wang Q, Ahn Geun H, et al. MoS2 transistors with 1-nanometer gate lengths. Science. 2016;354(6308):99-102.

27.Radisavljevic B, Radenovic A, Brivio J, Giacometti V, Kis A. Single-layer MoS2 transistors. Nat Nanotechnol. 2011;6(3):147-50.

28.Liang J, Xu K, Toncini B, Bersch B, Jariwala B, Lin Y-C, et al. Impact of Post-Lithography Polymer Residue on the Electrical Characteristics of MoS2 and WSe2 Field Effect Transistors. Advanced Materials Interfaces. 2019;6(3):1801321.

29.Jo I, Pettes MT, Kim J, Watanabe K, Taniguchi T, Yao Z, et al. Thermal conductivity and phonon transport in suspended few-layer hexagonal boron nitride. Nano Lett. 2013;13(2):550-4.

30.Zhang K, Feng Y, Wang F, Yang Z, Wang J. Two dimensional hexagonal boron nitride (2D-hBN): synthesis, properties and applications. Journal of Materials Chemistry C. 2017;5(46):11992-2022.

31.Pizzocchero F, Gammelgaard L, Jessen BS, Caridad JM, Wang L, Hone J, et al. The hot pick-up technique for batch assembly of van der Waals heterostructures. Nat Commun. 2016;7:11894.

32.Zomer PJ, Guimarães MHD, Brant JC, Tombros N, van Wees BJ. Fast pick up technique for high quality heterostructures of bilayer graphene and hexagonal boron nitride. Applied Physics Letters. 2014;105(1):013101.

33.Liang S-J, Cheng B, Cui X, Miao F. Van der Waals Heterostructures for High-Performance Device Applications: Challenges and Opportunities. Advanced Materials. 2020;32(27):1903800.

34.Kwon J, Shin J-C, Ryu H, Lee JY, Seo D, Watanabe K, et al. Multioperation-Mode Light-Emitting Field-Effect Transistors Based on van der Waals Heterostructure. Advanced Materials. 2020;32(43):2003567.

35.Lee GH, Cui X, Kim YD, Arefe G, Zhang X, Lee CH, et al. Highly Stable, Dual-Gated MoS2 Transistors Encapsulated by Hexagonal Boron Nitride with Gate-Controllable Contact, Resistance, and Threshold Voltage. ACS Nano. 2015;9(7):7019-26.

36.Xue J, Sanchez-Yamagishi J, Bulmash D, Jacquod P, Deshpande A, Watanabe K, et al. Scanning tunnelling microscopy and spectroscopy of ultra-flat graphene on hexagonal boron nitride. Nat Mater. 2011;10(4):282-5.

37.Wang Y, Chhowalla M. Making clean electrical contacts on 2D transition metal dichalcogenides. Nature Reviews Physics. 2022;4(2):101-12.

38.Zheng Y, Gao J, Han C, Chen W. Ohmic Contact Engineering for Two-Dimensional Materials. Cell Reports Physical Science. 2021;2(1):100298.

39.Cui X, Lee G-H, Kim YD, Arefe G, Huang PY, Lee C-H, et al. Multi-terminal transport measurements of MoS2 using a van der Waals heterostructure device platform. Nature Nanotechnology. 2015;10(6):534-40.

40.Jain A, Szabó Á, Parzefall M, Bonvin E, Taniguchi T, Watanabe K, et al. One-Dimensional Edge Contacts to a Monolayer Semiconductor. Nano Letters. 2019;19(10):6914-23.

41.Moon BH, Han GH, Kim H, Choi H, Bae JJ, Kim J, et al. Junction-Structure-Dependent Schottky Barrier Inhomogeneity and Device Ideality of Monolayer MoS2 Field-Effect Transistors. ACS Applied Materials & Interfaces. 2017;9(12):11240-6.

42.Yang Z, Kim C, Lee KY, Lee M, Appalakondaiah S, Ra C-H, et al. A Fermi-Level-Pinning-Free 1D Electrical Contact at the Intrinsic 2D MoS2–Metal Junction. Advanced Materials. 2019;31(25):1808231.

43.Son J, Kwon J, Kim S, Lv Y, Yu J, Lee J-Y, et al. Atomically precise graphene etch stops for three dimensional integrated systems from two dimensional material heterostructures. Nature Communications. 2018;9(1):3988.

44.Jung Y, Choi MS, Nipane A, Borah A, Kim B, Zangiabadi A, et al. Transferred via contacts as a platform for ideal two-dimensional transistors. Nature Electronics. 2019;2(5):187-94.

45.Decker R, Wang Y, Brar VW, Regan W, Tsai HZ, Wu Q, et al. Local electronic properties of graphene on a BN substrate via scanning tunneling microscopy. Nano Lett. 2011;11(6):2291-5.

46.Wu C, Soomro AM, Sun F, Wang H, Huang Y, Wu J, et al. Large-roll growth of 25-inch hexagonal BN monolayer film for self-release buffer layer of free-standing GaN wafer. Sci Rep. 2016;6:34766.

47.Shi Y, Hamsen C, Jia X, Kim KK, Reina A, Hofmann M, et al. Synthesis of few-layer hexagonal boron nitride thin film by chemical vapor deposition. Nano Lett. 2010;10(10):4134-9.

48.Xu ZQ, Elbadawi C, Tran TT, Kianinia M, Li X, Liu D, et al. Single photon emission from plasma treated 2D hexagonal boron nitride. Nanoscale. 2018;10(17):7957-65.

49.Villena M A HF, Liang X H, Shi Y Y, Yuan B, Jing X, Zhu K C, Chen S C and Lanza Variability of metal/h-BN/metal memristors grown via chemical vapor deposition on different materials
Microelectron Reliab 2019;102.

50.Choi S, Tran TT, Elbadawi C, Lobo C, Wang X, Juodkazis S, et al. Engineering and Localization of Quantum Emitters in Large Hexagonal Boron Nitride Layers. ACS Appl Mater Interfaces. 2016;8(43):29642-8.

51.Tran TT, Elbadawi C, Totonjian D, Lobo CJ, Grosso G, Moon H, et al. Robust Multicolor Single Photon Emission from Point Defects in Hexagonal Boron Nitride. ACS Nano. 2016;10(8):7331-8.
52.Chejanovsky N, Rezai M, Paolucci F, Kim Y, Rendler T, Rouabeh W, et al. Structural Attributes and Photodynamics of Visible Spectrum Quantum Emitters in Hexagonal Boron Nitride. Nano Lett. 2016;16(11):7037-45.
53.J KGaF. Efficient iterative schemes for ab initio total-energy calculations using a plane-wave basis set. Phys Rev B. 1996; 54 11169-86.
54.Perdew J P BKaEM. Generalized gradient approximation made simple. Physical Review Letters. 1996;77 3865-8.
55.KGaJD. From ultrasoft pseudopotentials to the projector augmented-wave method. Phys Rev B. 1999;59 1758-75.
56.E BP. Projector augmented-wave method. Phys Rev B Condens Matter. 1994;50 17953-79.
57.Kim S CMS, Qu D, Ra C H, Liu X, Kim M, Song Y J and Yoo W J Effects of plasma treatment on surface properties of ultrathin layered MoS2 2d Mater. 2016 3.
58.Kang S J K Y S JJH, Kwon J Y, Kim J H, Jung Y J, Kim J C, Kim B H, Bae S H, Huang P H, James Hone, Jeong H Y, Park J W, Lee C H, Lee G H Enhanced Photoluminescence of Multiple 2D van der Waals Heterostructures Fabricated by Layer-by-layer Oxidation of MoS2 ACS Appl Mater Interfaces 2021 13 1245–52.
59.Arenal R, Ferrari AC, Reich S, Wirtz L, Mevellec JY, Lefrant S, et al. Raman spectroscopy of single-wall boron nitride nanotubes. Nano Lett. 2006;6(8):1812-6.
60.Zhao Y, Wu X, Yang J, Zeng XC. Oxidation of a two-dimensional hexagonal boron nitride monolayer: a first-principles study. Phys Chem Chem Phys. 2012;14(16):5545-50.
61.Wu Q, Park JH, Park S, Jung SJ, Suh H, Park N, et al. Single Crystalline Film of Hexagonal Boron Nitride Atomic Monolayer by Controlling Nucleation Seeds and Domains. Sci Rep. 2015;5:16159.
62.Wang H, Zhang X, Liu H, Yin Z, Meng J, Xia J, et al. Synthesis of Large-Sized Single-Crystal Hexagonal Boron Nitride Domains on Nickel Foils by Ion Beam Sputtering Deposition. Adv Mater. 2015;27(48):8109-15.
63.Raidongia K JD, Upadhyay-Kahaly M, Waghmare U V, Pati S K,. Synthesis, structure and properties of homogeneous BC4N nanotubes J Mater Chem 2008;18 83-90.
64.Matsoso B J RK, Mutuma B K, Lerotholi T, Jones G and Coville N J. Synthesis and characterization of boron carbon oxynitride films with tunable composition using methane, boric acid and ammonia New J Chem 2017 41 9497-504.
65.McDougall N L PJG, Nicholls R J, Russo S P and McCulloch D G Influence of point defects on the near edge structure of hexagonal boron nitride Phys Rev B 2017 96.
66.S SMSaXD. Magnetic properties of vacancies in a graphitic boron nitride sheet by first-principles pseudopotential calculations Phys Rev B 2007 75.
67.Zobelli A, Gloter A, Ewels CP, Seifert G, Colliex C. Electron knock-on cross section of carbon and boron nitride nanotubes. Physical Review B. 2007;75(24).
68.Jin C, Lin F, Suenaga K, Iijima S. Fabrication of a freestanding boron nitride single layer and its defect assignments. Phys Rev Lett. 2009;102(19):195505.

69.Lee G H YYJ, Lee C, Dean C, Shepard K L, Kim P and Hone J Electron tunneling through atomically flat and ultrathin hexagonal boron nitride Appl Phys Lett 2011 99.

70.Kim D Y HN, Jeong H, Kim J, Hwang S and Kim J K Role of hydrogen carrier gas on the growth of few layer hexagonal boron nitrides by metal-organic chemical vapor deposition Aip Adv 2017 7.

71.Lawniczak-Jablonska K ST, Gorczyca I, Christensen N E, Attenkofer K E, Perera R C C, Gullikson E M, Underwood J H, Ederer D L and Weber Z L Electronic states in valence and conduction bands of group-III nitrides: Experiment and theory Phys Rev B 2000 61 16623-32.

72.Wang Y CM. Making clean electrical contacts on 2D transition metal dichalcogenides. Nature Reviews Physics. 2022;4(2):101-12.

73.Na YS, Kim JH, Kang S, Jeong JH, Park S, Kim DH, et al. Modulation of optical and electrical properties in hexagonal boron nitride by defects induced via oxygen plasma treatment. 2D MATERIALS. 2021;8(4).

74.Yeon H, Lin P, Choi C, Tan SH, Park Y, Lee D, et al. Alloying conducting channels for reliable neuromorphic computing. Nature Nanotechnology. 2020;15(7):574-9.

75.Wang H, Yan X, Wang S, Lu N. High-Stability Memristive Devices Based on Pd Conductive Filaments and Its Applications in Neuromorphic Computing. ACS Applied Materials & Interfaces. 2021;13(15):17844-51.

76.Moun M, Singh A, Singh R. Study of Electrical Behavior of Metal-Semiconductor Contacts on Exfoliated MoS2 Flakes. physica status solidi (a). 2018;215(14):1800188.

77.H. Ryu YL, H.-J. Kim, S.-H. Kang, Y. Kang, K. Kim, J. Kim, B. E. Janicek, K. Watanabe, T. Taniguchi, P. Y. Huang, H. Cheong, I.-H. Jung, K. Kim, Y.-W. Son, G.-H. Lee,. Anomalous Dimensionality-Driven Phase Transition of MoTe2 in Van der Waals Heterostructure. Advanced Functional Materials 2021;31, 2107376.

78.S. Shin SK, T. Kim, H. Du, K. S. Kim, S. Cho, S. Seo. Graphene transfer with self-doping by amorphous thermoplastic resins. Carbon 2017; 111, 215.

79.A. Pirkle JC, A. Venugopal, D. Hinojos, C. W. Magnuson, S. McDonnell, L. Colombo, E. M. Vogel, R. S. Ruoff, R. M. Wallace. The effect of chemical residues on the physical and electrical properties of chemical vapor deposited graphene transferred to SiO2. Applied Physics Letters 2011;99, 122108.

80.Lee G-H, Cui X, Kim YD, Arefe G, Zhang X, Lee C-H, et al. Highly Stable, Dual-Gated MoS2 Transistors Encapsulated by Hexagonal Boron Nitride with Gate-Controllable Contact, Resistance, and Threshold Voltage. ACS Nano. 2015;9(7):7019-26.

81.Cusati T FG, Gahoi A, Passi V, Lemme MC, Fortunelli A, et al. . Electrical properties of graphene-metal contacts. Scientific Reports. 2017;;7(1):5109.

82.Xia F, Perebeinos V, Lin YM, Wu Y, Avouris P. The origins and limits of metal-graphene junction resistance. Nat Nanotechnol. 2011;6(3):179-84.

Abstract in Korean (국문 초록)

전자 소자 응용을 위한 육방정계 질화붕소의 결함 연구

나윤성
공과대학 재료공학부
서울대학교

2차원 물질 중 넓은 밴드갭(5.5~6.0 eV)을 가진 육방정계 질화붕소는 우수한 절연 특성 때문에 전기 광학소자의 기판과 배리어 층으로 많은 연구가 진행되어 왔다. 최근에는 육방정계 질화붕소 내부에 존재하는 결함을 이용하여 싱글 포톤 에미터나 멤리스터 같은 메모리 소자에 관한 연구가 조명을 받고 있다. 이처럼 결함의 생성과 제어는 2차원 물질의 전기광학적 특성을 결정하는데 중요한 인자이다. 그러나 결함이 재료 특성을 결정하는 중요한 인자임에도 불구하고 결함에 의해 나타나는 육방정계 질화붕소의 전기광학적 특성 변화에 대한 연구는 미흡하다.

본 논문에서는 산소 플라즈마 장비를 이용하여 육방정계 질화붕소에 결함을 형성시켜 결함에 의한 전기적 광학적 특성변화를 다양한 측정 방법으로 관찰하였다. 325nm 파장의 레이저를 가진 라만 측정 장비로 photo luminescence(PL)를 확인하여 다양한 종류의 결함의 생긴 것을 확인하였다. DFT 계산을 통해 결함의 종류를 확인하고 PL 측정값과 매칭시켰다. 또한, 산소 플라즈마에 의해 형성된 결함 패스는 hBN의 밴드갭을 5.7 eV에서 4.5 eV까지 감소시켰다.

2차원 물질은 대기 중에서 산소와 수분 등에 의해 쉽게 산화되거나 데미지를 받는다. 이런 이유로 2D 물질을 이용한 전기 광학소자는 소자의 안정성을 위해 패시베이션 공정이 필수적이며 육방정계 질화붕소는 2D 소자의 이상적인 패시베이션 재료로 사용되어 왔다. 패시베이션 공정

으로 인해 2D 소자는 컨택 공정을 통해 메탈과 채널을 연결시켜야 한다. 우리는 hBN으로 인캡된 그패핀과 MoS2 소자를 제작하여 전기특성을 확인하였다. 산소 플라즈마 처리를 통해 hBN에 결함을 형성시키고 반복적이 전압 인가를 통해 메탈과 채널 사이에 전도성 패스가 형성하였다. 결과적으로 전도성 패스를 이용한 소자는 기존 보고된 소자와 동등한 전기적 특성을 보여주었다. 우리의 연구 결과는 이상적인 2D 소자를 구현하는데 있어 유용하고 새로운 컨택 공정을 제시하였다.

주제어 : 육방정계 질화붕소, 산소 플라즈마, 2D 전자 소자, 전도성 패스, vdW 헤테로구조